

Sergio DeSouza-Machado,
Department of Physics,
University of Maryland Baltimore County,
1000 Hilltop Circle,
Baltimore MD 21250

November 19, 2019

Dr. Lars Hoffmann,
Associate Editor,
Atmospheric Measurement Techniques

Dear Dr. Hoffmann,

This cover letter is included with the submission of our revised paper (amt-2019-282) entitled

“kCARTA : A fast pseudo line-by-line radiative transfer algorithm with analytic Jacobians, fluxes,
Non-Local Thermodynamic Equilibrium and scattering for the infrared”

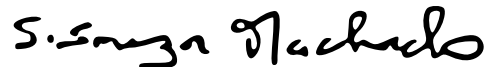
together with our responses to the reviewers.

In writing the manuscript, as before we have adhered as strictly as possible to the AMT manuscript guidelines. This document includes

- Page 1 : this cover letter,
- Page 2 : preamble for responses to reviewers,
- Pages 3-10: point-by-point response to Reviewer 1 (submitted earlier today as amt-2019-282-AC1-supplement.pdf),
- Page 11 : point-by-point response to Reviewer 2 (submitted earlier today as amt-2019-282-AC2-supplement.pdf),
- Pages 12-13 : point-by-point response to Reviewer 3 (submitted earlier today as amt-2019-282-AC3-supplement.pdf),
- Pages 14-15 : list of relevant changes from the above point-by-point responses,
- Pages 16-45 : output from latexdiff between the original and revised manuscripts

I have also separately uploaded the revised manuscript to AMT. We are confident we have taken great care to address all the concerns of the three referees, and look forward to your favorable response. Should you need to contact me, my email address is sergio@umbc.edu.

Sincerely,



Sergio De Souza-Machado

kCARTA : A fast pseudo line-by-line radiative transfer algorithm with analytic Jacobians, fluxes, Non-Local Thermodynamic Equilibrium and scattering for the infrared

by DeSouza-Machado et. al.

We thank the anonymous referees for their detailed read of the paper and providing introspective comments, many of which have resulted in changes to the revised version of the manuscript. In particular we have improved the accuracy of the computed kCARTA radiances by changing our default options (now linear-in-tau, higher resolution spectral database in the 15 um region). This update has already been pushed to github. We have also shortened the paper by removing the sections describing comparisons between the HITRAN/GEISA/CO₂ line-mixing databases, and the impact of spectroscopic uncertainties on TOA radiances. This has been replaced by a section where we compare kCARTA versus LBLRTM TOA radiances. Below we detail our responses to their individual concerns. For ease of review, we type-faced the reviewers questions in blue. When we refer to pages and line numbers in our answers, the context should make it clear whether we are talking about the original manuscript or our current revised manuscript.

Specific comments

1) There is no comparison of kCARTA radiances with a more well-established (and preferably line-by-line) model, not even the source models UMBC-LBL or LBLRTM. The kCompressed tables have been previously verified to reproduce the absorption coefficients or optical paths, but this paper deals with all the extra components of a radiative transfer model.

We have added a section that describes detailed inter-comparisons against LBLRTM.

2) I have concerns about the impact of the coarse spectral resolution: 0.0025cm^{-1} . Where does this figure come from? The usual requirement for radiative transfer is to be able to capture the signal from Doppler-broadened lines in the upper stratosphere, which have typical mid infrared widths of 0.001 cm^{-1} , hence resolutions of 0.0005 or 0.001 cm^{-1} are generally considered necessary. Given the inherent flexibility of the kCompressed tables, I am also surprised that the authors have not considered using an adaptive, rather than fixed, spectral grid, so that the spectral resolution is concentrated around the line-centers, so obtaining better accuracy for the same size compressed datasets and computation time.

As clearly stated in the title and abstract of the manuscript, kCARTA is a pseudo (monochromatic) line-by-line code, written specifically to compute radiances which are accurate when convolved with the Spectral Response Functions of the new generation of hyperspectral nadir sounders (or larger than 0.1 cm^{-1} resolution). The loss of information due to compression with a finite number of basis vectors, means that for some molecules with complicated lineshapes we cannot completely reproduce the true monochromatic optical depths. However after convolution with a typical sounder response functions (resolution typically 0.5 cm^{-1} at $15\text{ }\mu\text{m}$), kCARTA is shown to easily compute accurate radiances (especially keeping in mind the large spectroscopic uncertainties that still exist in CO_2 line mixing, and larger detector NeDT at the long wavelengths, see for example Figs 3,4,5 of the original manuscript). We have re-written parts of the Paragraph 1, Page 2 to emphasize this.

We also thank the reviewer for pointing out we can easily improve kCARTA inter-comparisons against for example LBLRTM by changing the defaults to be (a) linear-in-tau and (b) higher resolution at the $15\text{ }\mu\text{m}$ region ($605\text{-}880\text{ cm}^{-1}$). The above mentioned additional section will demonstrate we have tested and implemented this; any user interested is using higher resolutions can easily do so, by generating the appropriate database.

We have previously explored constructing and using databases of lower resolution in the lower atmosphere, and gradually increasing the resolution as the layer pressure decreases, but we found that while we could retain the TOA accuracy, the code was slowing down. More importantly the SVD compression works best with single resolution. The compressed files are small enough that it does not matter if the resolution is higher than needed in the troposphere.

3) I am unclear on the conversion of atmospheric profile quantities (temperature, pressure, composition) to the (presumably?) equivalent homogeneous paths represented by the kCompressed data. Are these absorber-weighted equivalent (ie Curtis-Godson) temperatures and pressures? Or simply layer means? Given the use of a spherical atmosphere (what radius of curvature is assumed?) rather than a plane-parallel assumption, presumably some sort of numerical integration scheme is required to obtain these quantities, even the total amount of absorber in a layer.

Line 455 of the original manuscript states that our kLAYERS program takes in n -level point profiles (typically pressure, temperature, water vapor and ozone profiles), interpolates these points onto a fine grid and then integrates to produce the final integrated layer output profiles for the gases (in molecules/cm²) and one average temperature (same for all gases) at each of the AIRS 100 layers. We wanted to define one layer temperature for all gases, as kCARTA (and SARTA) are used for atmospheric retrievals. Furthermore kCARTA is effectively monochromatic, so does not need Curtis-Godson temperatures.

Internally kCARTA does have the ability to use individual (Curtis-Gordon) gas temperatures at each layer, but those need to be provided as input.

The kLAYERS program uses Planet Earth parameters (radius and height dependent gravity), and also adds in the variable trace gas profiles as needed (such as CO_2 , CH_4 , CO). The kCompressed database is saved at the same AIRS 100 layers, so the default kCARTA ingests the output of kLAYERS, un-compresses the

database and does the radiative transfer.

4) Section 4, on the impact of spectroscopy on TOA radiances, seems an unnecessary digression. While spectroscopic uncertainties are certainly an issue that merits attention, that's not really anything to do with the kCARTA model being introduced (besides which all the variation is handled in the generation of the kCompressed datasets, which are to some extent independent). The data gap in the plots, arising from the gap in AIRS coverage, is also undesirably for such a comparison. It would have been more useful to see comparisons of kCARTA TOA radiances against other models instead.

Showing TOA BT uncertainties due to spectroscopy is very important, both for scientists working on retrievals and for those working on data assimilation. To our knowledge this assessment has not been documented (at least recently). However we agree it is an unnecessary digression in this paper, and have removed the entire Section 4 of the original submission.

5) For most molecules, kCARTA uses data created by the UMBC-LBL model using the Van Vleck and Huber lineshape. Since the Voigt lineshape is very much the 'standard', there should be some explanation of how this differs and why it is used in preference to Voigt.

UMBC-LBL is based on GENLN2, which also uses the Van Vleck/Huber lineshape. Initially used with Lorentz lineshapes to model microwave absorption, our implementation is a sum over two voigt lineshapes, one centered at v_0 and the other centered at $-v_0$. The VVH lineshape would have larger impacts for the microwave regions; for the infrared wavelengths considered here the second term is negligible and it is essentially the Voigt lineshape.

6) The inclusion of non-LTE effects, just for the CO₂ 4um band, seems to require the inclusion of a separate line-by-line model within kCARTA. This is a huge overhead in complexity for a relatively specialized application. Given the kCARTA structure, it seems a more natural approach would have been to incorporate vibrational temperature as an extra axis on the kCompressed datasets, and just use GENLN2 to calculate these. Alternatively, if you are including a LBL model within kCARTA, at least extend it so that LBL (with or without non-LTE) can be used for any molecule.

We have already included links to our monochromatic (Matlab based) LBL code. For nadir sounders that kCARTA is designed for, we only need 4 μm CO₂ NLTE effects where the different vibrational temperatures means we need to account for both the changes in optical depths and for the modifiers to the Planck function. The existing code inside kCARTA can compute both NLTE and LTE effects (for the 4 um CO₂ lines for which we include line and line-mixing parameters), but since we do not use accelerated Voigt functions or continuums, using it for all molecules would unnecessarily slow down kCARTA. We have explored making a NLTE compressed look-up scheme for kCARTA, for both the optical depths and multipliers to the Planck function. However we did not get satisfactory results, and left this as a "to be revisited someday" project.

7) The calculation of background thermal radiation (section 7) uses an interesting idea, and would probably have merited some expansion as a separate (if somewhat specialized) article by itself. I have a number of questions, detailed in the minor comments

We have answered those questions.

TYPOS/MINOR COMMENTS

P1 L20: '... data are presently ...'

Fixed

P1 L20: Given Susskind was describing cloud clearing for the previous generation of meteorological instruments I'm not sure it's an appropriate reference for the hyperspectral instruments.

The previous generation of weather sounders included HIRS. AIRS is the first of the new generation of hyperspectral sounders. The referenced 1998 Susskind paper is the most relevant reference for operational cloud clearing, and it discusses retrievals using simulated AIRS spectra.

P1 L20: The text may be read as implying that there is some sort of correction applied to the spectra to remove the influence of clouds, whereas I suspect it is more accurate to say that any cloud-contaminated spectra are simply rejected.

With ~ 15 km footprints, less than 4% of current hyperspectral sounder observations can be identified as mostly cloud free. The $\geq 60\%$ global coverage retrieval yield of the operational NOAA CrIS NUCAPS and NASA AIRS L2 retrievals is achieved by explicitly using cloud cleared radiances.

P2 L27: What determines this 0.0025cm^{-1} figure? As a rough estimate I expect it would be determined by the requirement to resolve the Doppler widths of lines, and given molecular velocities are of the order of $c/10^6$ that would correspond to around 0.001 cm^{-1} at 1000 cm^{-1} .

As noted at the beginning, and is explicitly part of the new Section 7 in the revised manuscript, the key requirement is that the monochromatic kCARTA radiances can be accurately compared to any real (or hypothetical) sounder radiance. This is achievable using a database generated at 0.0005 cm^{-1} , five point box car generated to 0.0025 cm^{-1} . However to further improve the accuracy, we have changed the resolution of kCARTA to be 0.0005 cm^{-1} in the $605\text{-}880\text{ cm}^{-1}$ region. If required kCARTA can easily switch to use higher resolution databases across any spectral range, which now are much faster to generate.

P2 L27: I am not convinced by the argument that the computation of optical depths at high spectral resolution for 50 or so profiles for the training set is something that needs accelerating. Surely this is something that only has to be done once and, even if occasionally repeated, the fact that it takes a week rather than a couple of hours isn't really be an issue.

Our historical motivation has been further explained in Q2 above. kCARTA is also used to check the newly developed (and/or existing) fast model against tens of thousands of other regression profiles we have, as well as tens/hundreds of thousands of AIRS, CrIS and IASI observations as needed. All this can be done extremely rapidly in an embarrassingly parallel fashion with kCARTA. We also generate monochromatic jacobians and weighting functions for some of these observations or test profiles, which for the $605\text{-}2830\text{ cm}^{-1}$ region can be done by kCARTA in less than two additional minutes per profile.

P2 L40: I assume the issue with replacing line-by-line with kCompressed data is one of the accuracy of the absorption coefficient or reconstructed layer optical depths. However to state that the 'radiances' are accurately reproduced requires a whole new set of tests to verify the accuracy of the radiative transfer through an atmosphere.

Our 1998 paper stresses we tested the accuracy of the reconstructed radiances against those computed using the uncompressed monochromatic tables. Plus we regularly perform a number of tests offline, involving both single gas and multiple gas radiative path integrals. We hope answers/revisions made to the manuscript further address some of this.

P2 L49: Missing second ')' after 1999.

Fixed

P3 L71: I have not come across the Van Vleck and Huber lineshape. Is this different to the more conventional Voigt? If so, how, and why the unconventional choice?

As explained above, for the infrared it is essentially the Voigt lineshape.

Fig 1: I appreciate this is just a sketch, but the black Total line doesn't seem to be a sum of the red, blue and green lines. Also raise the '-1' in the x-axis title to a superscript (and in subsequent figures).

We have fixed the xlabel here and in other places. Regarding the sums, we checked that everything is OK by modifying the code that generated this plot to print out the y - values of the blue, green and three red curves at various points inside the $x \in (-0.5, +0.5)$ interval, the sum of these values, and the y - value of the black curve, and verified they were identical.

P4 L98: Regarding MonoRTM - what is the point being made here?

Our understanding is that monoRTM is the reference line-by-line code which LBLRTM is checked against. So, our compressed ODs are as accurate as the monoRTM ODs (at least for $10\text{ }\mu\text{m}$ O_3 absorption spectrum), and we are confident the Van Vleck/Huber lineshape in the UMBC-LBL code will work just as accurately when used for appropriate molecules in the IR region (this would obviously not be true for molecules that use specialized lineshapes, such as CO_2 and CH_4 linemixing). Since that point did not come across clearly, and is not really needed, we have removed it.

P5 L107: +/- 50K does not seem a large range in temperature. Do you have any evidence that it spans

the full range of atmospheric variability?

We read in one set of ECMWF data for 2019/08/01 (360x180 one degree grid points) and ran the ~ 64000 profiles through kLAYERS. All but 4% of the temperature profiles lay within ± 50 K of the US Standard temperature profile. The ones that lay outside these bounds were all profiles over the Antarctic plateau, on average 3 ± 2 K outside the -50 K offset (between 500 - 1000 mb). kCARTA handles these cases by extrapolating compressed ODs (and zero checking) as needed. We have added this information into the appropriate place of the revised manuscript using the following phrases “Tests using NWP profiles show this is usually sufficient everywhere except for a handful over the winter Antarctica, which could fall slightly outside the coldest offset (on average by about 3 K) between 600-1000 mb; kCARTA handles these cases by extrapolating what has been compressed.”

P5 L108: 'contains'

Fixed

P5 L122: HITRAN 2016 lists two further isotopologues for water vapour containing a single deuterium atom and either a ^{17}O or an ^{18}O oxygen isotope (these are HITRAN isotopologues 5 and 6). Are these included with HDO or with the remaining H₂O isotopologues?

With the remaining H₂O isotopologues

P6 L144: It is not clear why the cross-section molecules are also represented using kCompressed databases. Presumably these end up much larger than the original files, which usually have only a few tens of (pressure,temperature) points and a much coarser spectral axis. Also using CIA probably won't work with LUTs - how will these new data be used?

We chose to do it this way in order to compute the ODs of all gases (molecular and cross-section) equally. In any case our database size is dominated by the main molecular gases (H₂O, CO₂, O₃). The CIA is handled by calling the necessary routines within kCARTA.

P6 L150: HITRAN 2016 lists 49 rather than 42 molecules, and a number of these (or even 1:42) are not represented in the US Standard Atmosphere.

Correct, we only use the first 42 as we were able to get the “standard” or “realistic” profiles for them; similarly now HITRAN has very many cross sectional profiles but we only use the ones for which we are able to find representative profiles in the scientific literature.

We have amended the sentence to read “The default kCARTA mode is to use the 42 molecular gases in HITRAN database, together with about 30 cross-section gases, for which we have reference profiles. “

P6 L158: 'Schwarzschild'

Corrected

P7 Eq(3): The solid angle integration should just be over a hemisphere and should include the $B \cdot dt/ds$ term scaled by $\cos(e)$ where e is the elevation angle $0:\pi/2$ in the hemispheric integration (thus the integral of $\cos(e) \cdot d\Omega$ from $0:2\pi$ on its own should yield π).

Both fixed, thanks for pointing out these mistakes

P7 Eq(3): I don't see why the $\cos(\theta_{\text{sun}})$ appears in the last term on its own, but it seems there should be some solid angle integration over the sun's disk (as in Eq 6) otherwise it will be as if the whole sky radiates at the solar temperature.

The manuscript has defined $B_{\odot}(\nu)$ as the solar radiance at the TOA, so that accounts for the solar disk.

P7 L170: Isn't $1-\epsilon_s(\nu)$ the same as $\rho_s(\nu)$?

Default behavior of kCARTA is to do this; however we can explicitly input reflectivity so that we could for example handle sun glint off an ocean

P7 L171: extra comma near end of line

Fixed

P7 L171: There is no τ_i term in Eq(3), just τ and τ_{atm} .

Fixed

P7 L180: Assuming the temperature profile is specified at points P,H1,H2 etc what constant temperature is assumed for, eg the lowest layer? Is it T(P), T(H1), or something else?

Already answered above when we respond to the question regarding use of kLAYERS; it is the layer averaged temperature for the layer between P and $H1$

P7 L182: By 'density effects' do you mean refraction?

Correct

P7 L186: Both emissivity *and* reflectance have to be supplied? Eq(4) only uses emissivity.

Yes, Equations (3,6,7) shows that kCARTA also uses reflectivity. We have amended both sentences in that and subsequent sections to make it more clear.

P8 Eq(5): The indexing doesn't seem to work. Interpreting $\tau_{(i+1 \text{ to } N)}$ as the transmittance from the base of layer $i+1$ to the base of layer N the calculation for layer 3 in the diagram would be $(1 - \tau_{3,4}) \cdot \tau_{(4 \text{ to } N)}$ but here $N=4$ so $\tau_{(4 \text{ to } N)} = 1$ whereas it should be the transmittance through layer 4. Similarly Eqs 8-10

We see the confusion has arisen because we forgot to state that (a) τ_i represents the transmission through layer i (i.e. from bottom to top of layer i), and that (b) $\tau_{i+1 \rightarrow N}$ is the transmission from bottom of layer $i+1$ to top of layer N . So we have taken the opportunity to add in these definitions and make some additional clarifications in the relevant text/equations.

P8 L195 Better to swap sections 3.3 and 3.4 to match the same order these terms appear in Eq (3)

Done

P8 L196 rho is now defined as reflectance, but for Eq 3 it was reflectivity. Is there a difference?

We now consistently use reflectivity everywhere, instead of reflectance.

P9 L213 As a general comment, it would be nice to have a plot of the magnitude of these four terms as a function of the infrared spectrum, assuming say some fixed surface emissivity of around 0.98 (so 2% diffuse reflectance).

We added in a number of figures detailing the comparisons against LBLRTM, and decided not to do this.

P9 Section 4: Presumably for this exercise different sets of kCompressed databases were computed by running UMBC-LBL etc for the different sets of spectroscopic data, and then running kCARTA using these 3 different sets of kCompressed databases. If one really wants to demonstrate the differences in TOA radiance couldn't one simply run the LBL models with the different spectroscopic data and eliminate the whole intermediate step of generating kCompressed datasets?

We re-iterate that running the UMBC line-by-line code which does not use acceleration for the Voigt function and/or gas continuums is very time consuming, as it partitions the lines into "near" "medium" and "far". This has to be done molecule by molecule, layer by layer, across the entire 605-2830 cm^{-1} spectrum. This is a significant amount of time even if computed in embarrassingly parallel mode. Our 1998 JQSRT paper already shows how accurate our compressed database is. This means once the compression is done, kCARTA can be used to generate synthetic radiances for thousands of NWP model atmospheres in a number of minutes (when kCARTA is used in embarrassingly parallel mode).

P9 L230 'linemixing'

Fixed

P10 L243 'sagain' ?

Replaced with "panel"

P10 L247 it is not clear that differences have anything at all to do with linemixing - it seems they might simply reflect differences in the standard line widths that would be evident whether line-mixing effects were included or not?

That is possible, but we cannot exclude that differences in mixing coefficients determine how much intensity has to be transferred from the wings to the peaks. We have not investigated that idea as for now we have chosen to simply use available CO2 codes. A proper test would involve using other line-mixing codes together with different spectroscopic databases, but that is outside the scope of this paper.

P13 Section 5: It seems odd that kCARTA has a non-LTE line-by-line module - it is something I would have expected in the UMBC-LBL code. Have you considered modelling non-LTE using kCompressed datasets? That would seem more in keeping with the overall design. Perhaps you would need an extra tabulated dimension in vibrational temperature, or (vib-kin) temperature?

Our line-by-line code could indeed be modified to generate the ODs using the vibrational temperatures. However NLTE also effects the Planck function and we would also need to compute the multipliers to the Planck function and give them to kCARTA. For these and other reasons it is more natural to put the NLTE effects directly into the kCARTA RTA. As explained above, generating compressed lookup tables for NLTE effects remains a “to be revisited someday” project.

P13 Eq 9: Summations should be from $i=1,N$. Also, $\tau_{(i+1 \text{ to } N)}$ in second summation should have (nu) afterwards.

Fixed

P14 L304: 'Jacobian' from here to the end of the section start to be capitalised - inconsistent with earlier 'jacobian'

Fixed everywhere

PP14 L305: How is dB/dT calculated? (where $s.m = T.m$).

Analytic derivative of the Planck function

P14 L310: I don't understand the last sentence - what's the difference between the Jacobian and the weighting function wrt surface temperature and emissivity?

We have rewritten the sentence to state “kCARTA also computes the weighting functions, and jacobians with respect to the surface temperature and surface emissivity.”

P14 L320: 'contributes'

Fixed

P15 L334: the $d\mu$ should come after the $\exp(-x/\mu)$.

We have moved $\mu d\mu$ after the $\exp(-x/\mu)$

P14 L334: Is there any significance in labelling this integral as E.3 ?

It is the exponential integral of the third kind, and have added this to the text.

P14 L334: No closing bracket to match '('.

Fixed

P14 Eq 13: From discussing downward radiation, the introduction of reflectance ρ_s suggests to me that you are now modelling the reflected component of this radiance just above the surface. Where does the 2π come from? I think you need to explain some of the intermediate steps.

Assuming azimuthal symmetry when doing the hemispheric integral gives the factor of 2π .

P14 L340: If I understand this correctly, instead of approximating the downwelling radiance as if it comes from a fixed angle $\cos=3/5$, you are adjusting the angle for each atmospheric layer according to the surface-layer optical thickness x . It would be nice to see some plots of the comparisons with a full hemispheric integration to show that this is significantly more accurate than the fixed angle assumption. Also, is there a reason why the cut off at 30deg has to be applied for optically thick atmospheres? Otherwise it might also be useful for modelling the radiance viewed by upward-looking instruments, or downward looking instruments close to the surface.

LBLRTM does flux calculations at 3-4 gaussian quadrature angles, which is evidence that a single angle assumption is not accurate enough. Instead of this, we chose to do downwelling background thermal using a varying diffusivity angle at each layer. For optically thick regions, a TOA sounder is not going to remotely sense any contribution from the surface, whether it is directly emitted by the surface or reflected from the surface. Hence, in these regions there is no need to calculated the background thermal at all. We agree that for the more transparent regions, a little more care should be taken for downward looking instruments close to the surface, including a finer layering of the atmosphere closer to the surface, which kCARTA and kLAYERS can both handle, as discussed in the 1998 paper.

P15 L346: Given the rapid spectral variation in any 25cm-1 interval, I don't understand how you can assign a single assumption to the whole interval. Won't there be a whole range of optical thickness within the 25cm-1 region so that the assumption works better for some spectral points than others?

Both the lines and wings of an optically thick region are mostly opaque i.e. you do not go from transparent to optically thick in a few tenths of a wavenumber, but rather over an appreciable interval. So encompassing 25 cm⁻¹ chunks as we did is fine. Furthermore we have tested our assumption against Gaussian quadrature, and our method is far superior to simply using acos(3/5) for downwelling radiation. The user can also opt to use only acos(3/5) or do Gaussian quadrature.

P15 Sec 7.2: The linear-in-tau model, where optical depth is scaled by the sec(theta) to allow for off-nadir viewing angles, assumes a plane-parallel atmosphere where theta is fixed for the layer (and the same for every layer). How is this handled for the spherical atmospheres assumed in kCARTA where cos(theta) can vary significantly when viewing off-nadir?

kCARTA defaults to dividing an 80 km thick atmosphere into about 100 layers, with the layers starting out being about 0.25 km thick at the bottom, and gradually increasing in thickness the higher you go. The linear-in-tau models the temperature variation through each of the individual layers. So kCARTA does linear-in-tau T(tau(i)) at angle theta(i) the same way as it does constant T(i) at angle theta(i) : by varying the angle layer by layer as the beam propagates upwards.

P16 L365: It depends what you mean by the 'average layer temperature'. For the optically thin limit you would expect this to converge to the Curtis-Godson temperature, ie the absorber-weighted mean temperature, which would generally be at an altitude below the layer mid-point.

As explained above, we accurately determine the mean layer temperature using kLAYERS, and then use the definitions in the Clough et al 1992 JGR paper to determine the temperature variation across the layer.

P16 L377: Even though it largely disappears after convolution (presumably because the AIRS spectral resolution means that the radiance is dominated by contributions from lower altitudes), this 10 K difference does seem to be a serious issue. And one which would limit the use of kCARTA for accurately representing finer resolution instruments. Is this really due to not implementing linear in tau or could it be that kCARTA only uses a crude representation of layer temperature rather the something more physically justified such as Curtis Godson temperature? Why doesn't kCARTA just use the linear-in-tau model?

Given an input temperature profile, kLAYERS internally interpolates to a fine grid before accurately finding the mean layer temperature. We do not need a Curtis-Gordon temperature since at each wavenumber point we are essentially monochromatic (not a band model). It is also well known that hyperspectral sounders have at most about 12-15 degrees of freedom for temperature, so our 100 layers are more than adequate. We also input the kLAYERS temperature profile into the LBLRTM TAPE5, and as far as we can tell it is then not using a more physically justified temperature than kCARTA does.

As mentioned in the title and at the beginning of the answers, kCARTA is a pseudo (monochromatic) line-by-line code. The large (10+ K) differences are seen when comparing kCARTA to LBLRTM at 0.0025 cm⁻¹ resolution, since the latter internally is doing the upper atmosphere calculations at high resolution. As we improve the kCARTA database resolution, the differences become significantly smaller. For example if we use 0.0002 cm⁻¹ resolution, it drops to less than 1 K ± 1 K right on top of the high altitude 15 μm CO₂ lines, and -0.1 ± 0.05 K in the high altitude O₃ sounding channels, when averaged over our 49 regression profiles. If we use 0.0005 cm⁻¹ resolution, the 15 μm/10 μm numbers are correspondingly 4 ± 1 K and -0.3 ± 0.1 K. After convolution with a sounder SRF, the differences are negligible. As mentioned earlier, we thank the referee for pointing this out to us and have made 0.0005 cm⁻¹ the default resolution in the thermal IR; any interested user can easily generate and use a higher resolution grid if desired.

We note that it appears that we run into slight differences in CO₂ line broadening and/or resolution right on top of the lines, and perhaps algorithm differences (LBLRTM may use a Pade approximation and/or Eqn 15/16 to first order while we use Eqn 16 to fifth order).

The above evidence provides ample confidence that the linear-in-tau RTA is working quite well, even when allowing for ray tracing. As expected after convolution with a sounder SRFs, these differences mostly vanish, since these differences are right at the peaks of a small number of very high sounding CO₂ lines.

This is all described in the (new) section 7, on inter-comparing kCARTA and LBLRTM. We note this meant

we also had to change a few sentences in the section on flux computations, and in Appendix B. kCARTA now uses the linear-in-tau model.

P17 L390 'computes'

Fixed

P17 Flux Computations: are these with spherical or plane-parallel atmospheres?

Whether you use the (exponential or legendre) gaussian quadrature, we use the same fixed quadrature points at each layer so that is plane parallel.

P17 L407: Given the differences found from the linear-in-tau model in the previous section, could the differences in heating rates at high altitude simply be another manifestation of the same problem, ie assumption of constant temperature within thick layers at higher altitudes?

We believe our above responses above adequately address this issue, namely it is the resolution. In addition we have stated when doing flux computations, kCARTA uses linear-in-tau.

P18 Fig 6 caption: should be '0.0005' instead of '0.005'.

Fixed

P18 L425: 'accuracy of its spectroscopic database'. I assume this refers to the kCompressed tables used as kCARTA input as opposed to the usual meaning which would be HITRAN or GEISA spectroscopic databases. But comparisons against GENLN2 or LBLRTM wouldn't just be a comparison of the kCompression with the original HITRAN unless your tests were for simple homogeneous paths where transmittance could be verified independently of other model assumptions such as ray-tracing and integration through atmospheric layers.

Correct we are referring to the accuracy of the compression.

P19 L434: '0.0025 cm-1 is good enough for nadir hyperspectral sounders' - this is a contentious statement, and needs some justification (there is none in this paper).

We are confident our responses to the earlier questions address this issue, especially in light of the fact that most residuals are far smaller than detector NeDT when the radiances are convolved with realistic sounders response functions.

P21 Table B2: lists (6) Direction as downwelling by default, upwelling as an option. Isn't it the other way around?

Corrected, thanks for pointing this out

P22 L488: extra ')'

Fixed

P22 L495: 'up to'

Fixed

Specific comments

1). What studies have the authors done to ensure that the 11 temperature grid points are adequate to represent the temperature dependency of optical depths of gases for each atmospheric layer. Please quantify the errors of interpolation due to 11 point grid and the choice of interpolation method (spline vs linear).

We have addressed the first part of this question above. The spline versus linear interpolation errors work out to be 0.0004 ± 0.0040 K when averaged over all monochromatic spectral points, for 49 regression profiles, with a maximum absolute difference of 0.342 K (in the 15 μm region). This information has been inserted into Appendix B of the revised manuscript.

2). The kCARTA package is optimized for the thermal infrared spectral region. Though the authors claim it is trivial to extend the database out to span the far infrared to ultra-violet range, the package does not include Rayleigh scattering and an accurate multiple scattering radiative solver, which are important for the shortwave top of atmosphere radiation calculations.

Correct, we have fixed Section 9 and Appendix to state that PCLSAM is optimized for the thermal infrared away from solar scattering effects, so we have codes to read in ODs uncompressed by kCARTA for arbitrary atmospheres, which can then be passed to for example LBLDIS.

3). On page 2 line 40, it will be useful to describe the relative errors between kCarta and the MNLBL.

The UMBLBL code computes only optical depths, and does not have any radiative transfer computations. As mentioned above and in the next question, we have added a section that describes detailed top-of-atmosphere radiance intercomparisons against LBLRTM.

4). Section 2.1 on page 4. Although the authors described the UMBC-LBL model line shape calculations and mentioned that extensive comparisons with LBLRTM and GENLIN2 have been performed, no quantitative results have been shown to illustrate differences among different LBL models. For some molecules, a sub-Lorentz line shape is used by LBLRTM, what about the UMBC-LBL?

As asked by two reviewers, we have added a section that describes detailed inter-comparisons against LBLRTM. We are also happy to provide interested users with a database generated entirely using the optical depths in LBLRTM.

5). The method used by kCARTA for calculating the downwelling background radiative is very efficient and much more accurate relative to a constant diffusive angle. However, for a non-Lambertian surface (e.g a specular reflection surface), this may not be a good approximation.

Correct, an example BRDF for sunglint is modeled in Appendix A of the Nalli et. al 2016 paper we have referenced.

There are some minor errors in the manuscript:

1. In the figure caption for Figure 6, 0.005 cm^{-1} should be 0.0005 cm^{-1} .

Fixed

2. Not all the symbols used in this paper are defined. For example, Ω in equation (3), g under equation (C1). . .

Fixed

3. Some of the links given in Appendix A are not available.

Fixed the line-by-line code link to point to https://github.com/sergio66/UMBC_LBL. The others were valid/accessible.

4. Line 149, the symbols in the equation are not explained by the text or the appendix B.

Fixed

5. Line 230, please correct typo “limemixing”

Fixed

Reviewer 3

Specific comments

1) This paper describes a particular incarnation of kCARTA which the authors are making available. It would be very helpful to have a version identifier for the version described in the paper, and perhaps further identification, if possible, of which previous versions have been widely used. This is particularly needed in the paragraph beginning at Line 132, where the phrase “we now use” is unclear as to which previous version is obsolete.

In Appendix A we now explicitly mention that SRCv1.21, together with HITRAN 2016 and LBLRTM12.8 for CO₂,CH₄ is used for the latest coefficients for the SARTA v2.01 (2019) versions for AIRS, CriS and IASI. In the same location we also clarify that we generate a new compressed database every 4 years (roughly within a year of a new HITRAN release)

Typographical errors:

Line 28, add comma after “process”

Fixed

Line 59-60, mismatched parentheses

Fixed

Line 158, “Schwarzschild” is misspelled

Fixed

Line 163, “radiation propagating” are both misspelled

Fixed

Line 171, remove the extra comma

Fixed

Line 242, unmatched bracket

Fixed

Line 243, “again” misspelled

Fixed

Line 322, remove comma after “i”

Fixed

Line 334, mismatched parentheses

Fixed

Line 335, coming “from” all

Fixed

Line 493, “cloudy” should be “cloud”

Fixed

Line 536, “A.B.” should be Boynard, A.

Fixed

Line 536, “P.M.” should be Pommier, M.

Fixed

Line 536, “A.R.” should be Razavi, A.

Fixed

Line 537, “Chenm” should be “Chem”

Fixed

Line 546, “Iacono” should be “Iacono”

Fixed

Line 580, “humidity” misspelled

Fixed

Line 584, list of authors is incomplete, at least add et al.

Fixed

Line 613, “I.E. G.” should be “Gordon, I.E.”

Fixed

Line 632, “Wm.” should be removed

Fixed

Line 649, “Karlsruhe”, not “Karlsruhr”

Fixed

Line 649, this link is dead. I find the paper at https://www.imkasf.kit.edu/downloads/SAT/kopra-docu_part02.pdf

Fixed

List of changes to manuscript

Here we list the changes to be found in the revised manuscript, and leave out fixes to typographical/spelling errors found in the original manuscript.

Major changes : The first two are the major changes, and are mentioned prominently in the abstract, introduction, Section 7 and conclusions.

- The default resolution of kCARTA is now 0.0005 cm^{-1} in the $605\text{-}880 \text{ cm}^{-1}$ region, and 0.0025 cm^{-1} in the $805\text{-}2830 \text{ cm}^{-1}$ region
- The default temperature variation is now “linear in tau”
- new Section 7 describes top-of-atmosphere Brightness Temperature intercomparisons between kCARTA and LBLRTM
- We have removed Section 4 from the original manuscript, which described the impact of spectroscopic uncertainties on synthetic top-of-atmosphere radiances

Changes/fixes in response to reviewer comments

- Section 2.2 (lines 115-118) : we describe the applicability of the $\pm 50 \text{ K}$ temperature offsets to realistic NWP model temperature profiles.
- Section 2.2 (lines 119-121) explicitly state the default resolution of kCARTA
- Section 2.2, (end, lines 160-165), we have added definitions of ν_0, T, m and clarified which gases are used in kCARTA
- Section 3, page 7-8 : we have fixed the equations and clarified some of the sentences describing the clear sky RTA in kCARTA
- Page 9, Sub-sections on background thermal and solar radiation have been swapped
- Equations in Section 5 (Jacobians) have been fixed, and some sentences clarified.
- Manuscript consistently uses reflectivity and emissivity everywhere
- Section 6.1, line 296 : Background thermal section defines $E_3(x)$
- Section 6.2 : Made some changes since kCARTA now uses default “linear in tau”
- Section 7 is a new section, describing in detail top-of-atmosphere brightness temperature differences between kCARTA and LBLRTM, as averaged over 49 regression profiles. The section describes these BTDs both monochromatically (as a function of varying database resolution), and after convolution with a typical hyperspectral sounder response function.
- Section 8 (flux comparisons) has been slightly changed since now we use as default a higher resolution database.
- Section 10 (Conclusions) has been slightly changed since we now use a higher resolution deep in the $15 \mu\text{m}$ region, and “linear in tau” temperature variation.
- Appendix A (code and database availability) has also been changed to reflect the above, and includes a short discussion of the version used to generate the current (2019) SARTA fast model database.
- Appendix B (kCARTA features) has been edited to reflect the above changes

- Appendix C (scattering) we now emphasize kCARTA does not have built in SW scattering ability, and suggest routines we have to output tables that can be read by for example LBLDIS. We have also made some changes to the text as requested by the reviewers.
- Acknowledgement section has been edited
- References should be free from mistakes.

kCARTA : A fast pseudo line-by-line radiative transfer algorithm with analytic Jacobians, fluxes, Non-Local Thermodynamic Equilibrium and scattering for the infrared

Sergio DeSouza-Machado¹, L. Larrabee Strow^{1,2}, Howard Motteler¹, and Scott Hannon³

¹JCET, University of Maryland Baltimore County, Baltimore, Maryland

²Dept of Physics, University of Maryland Baltimore County, Baltimore, Maryland

³Deceased

Correspondence: Sergio DeSouza-Machado (sergio@umbc.edu)

Abstract.

A fast pseudo-monochromatic radiative transfer package using a Singular Value Decomposition (SVD) compressed atmospheric optical depth database has been developed, primarily for ~~use with simulating radiances from~~ hyperspectral sounding instruments (~~resolution ≥ 0.1 cm⁻¹~~). The package has been tested extensively for clear sky radiative transfer cases, using field
5 campaign data and satellite instrument data. The current database uses HITRAN 2016 line parameters and is primed for use in the spectral region spanning 605 cm⁻¹ to 2830 cm⁻¹ (~~with a point spacing of 0.0025~~. ~~Optical depths for other spectral regions (15-605 cm⁻¹)~~), ~~but can easily be extended to other regions and 2830-45000 cm⁻¹~~ can also be generated for use by kCARTA . The clear sky radiative transfer model computes the background thermal radiation quickly and accurately using a layer-varying diffusivity angle at each spectral point; it takes less than ~~20-30~~ seconds (on a 2.8 GHz core using 4 threads) to complete a
10 radiance calculation spanning the infrared. The code can also compute Non Local Thermodynamic Equilibrium effects for the 4 μ m CO₂ region, as well as analytic temperature, gas and surface jacobians. The package also includes flux and heating rate calculations, and an interface to a scattering model.

1 Introduction

Recent years have seen the launch and routine operation of new generation infrared sounders on board Earth orbiting satellites,
15 for the purposes of providing measurements for data assimilation into Numerical Weather Prediction (NWP) centers and for monitoring atmospheric composition. These hyperspectral instruments have low noise channels with high resolution (~~≥ 0.5 cm⁻¹~~), and provide gigabytes of data daily, from about 620 - 2800 cm⁻¹. Examples include the Atmospheric InfraRed Sounder (AIRS)(Aumann et al., 2003) on board NASA's Aqua satellite, the Infrared Atmospheric Sounding Interferometer (IASI) on board the Metop satellites (Clerbaux et al., 2009) and the Cross Track Infrared Sounder (CrIS) on board the Suomi and JPSS-1
20 satellites (Han et al., 2013).

The radiances measured by these instruments are obtained under all-sky conditions (*i.e.* clear or cloudy). Publicly available thermodynamic profiles retrieved from this voluminous data ~~is are~~ presently performed *after* cloud-clearing the radiances

(Susskind et al., 1998). Monochromatic line-by-line (MNLBL) codes are too slow for use in the operational retrievals from the cloud-cleared radiances. Instead, optical depths (or transmittances) produced by these MNLBL codes are parametrized for use in fast Radiative Transfer Algorithms (RTAs), at the instrument resolution. The accuracy of the retrieved products depends on the accuracy of the fast models, which underlines the importance of the accuracy of line parameters and lineshapes used in MNLBL codes, particularly the far-wing effects.

~~Using MNLBL codes to produce optical depths for training the fast models is computationally intensive, as~~ To satisfy the accuracy requirements of convolved optical depths and radiances used in developing and testing these fast models, the high altitude (doppler broadened) lines need to have monochromatic spectral resolutions of 0.0025 cm^{-1} or better ~~are required~~ over the almost 2500 cm^{-1} span of a typical infrared sounder, ~~for~~. Using true MNLBL codes to produce optical depths for training the fast models is computationally intensive, as accurate lineshapes needed to be computed for millions of spectral points, each at about 100 layers spanning a 0-80 km atmosphere, for about 40-50 gases; this has to be done for 50 or more profiles. The acceleration of this part of the process, needed to develop a fast RTA for the AIRS sounder, was the motivating factor behind the development of the work presented here. For this we also developed a line-by-line code (referred to as UMBC-LBL) to produce an accurate pre-computed database of monochromatic atmospheric optical depths. Singular Value Decomposition (SVD) was then used to produce a highly compressed database (referred to as the kCompressed database (Strow et al., 1998)) that is highly accurate, relatively small, and easy to use. When coupled to an accurate radiative transfer code, ~~it~~ this pseudo line-by-line package can be used as a starting point for developing tools for atmospheric retrievals (Rodgers, 2000). The key point to note is that though some optical depth information may be lost due to the compression and/or resolution of the database, the convolved radiances are very accurate.

To compute optical depths and radiances at any level for an arbitrary Earth atmospheric thermodynamic + gas profile, we paired together an uncompression algorithm for the kCompressed database with a one dimensional clear sky radiative transfer algorithm (RTA). The RTA works for both a downlooking and an ~~up-looking~~ uplooking instrument, with geometric ray tracing accounting for the spherical atmospheric layers. The generation of monochromatic transmittances from the compressed database is ~~orders at least an order~~ of magnitude faster than using a MNLBL code; for the long paths in the atmosphere the computed transmittances are smooth and well behaved, and can be used to develop fast forward models. Radiances computed using the compressed database are as accurate as those computed with a MNLBL code as our compression procedure introduces errors well below spectroscopy errors (Strow et al., 1998).

The entire package is called kCARTA, which stands for “kCompressed Atmospheric Radiative Transfer Algorithm”. Although kCARTA *is* much slower than fast forward models which use effective convolved transmittances, it is much more accurate, and can be used to generate optical depths and transmittances for developing the faster models. An example is the Stand Alone Radiative Transfer Algorithm (SARTA) (Strow et al., 2003) for which kCARTA is the Reference Forward Model; SARTA is used to retrieve Level 2 geophysical products from the AIRS (Strow et al., 2003) and CriS (Gambacorta, 2013) instruments. Other fast forward models for the infrared which parametrize the transmittances of the finite width instrument channels include a Principal Component based Radiative Transfer Model (PCRTM; (Liu et al., 2006)), Radiative Transfer

for TIROS Operational Vertical Sounder (RTTOV; (Saunders et al., 1999)) and the Jülich Rapid Spectral Simulation Code (JURASSIC; (Hoffman and Alexander, 2009)).

60 kCARTA also includes algorithms to rapidly compute analytic jacobians, and is available in a Fortran 90 package. This package (v1.21, April 2019) uses some of the newer Fortran features such as implicit loops, function overloading and modules, and includes code for computing fluxes, heating rates, and the effects of cloud and aerosol scattering using the Parametrization of Clouds for Longwave Scattering in Atmospheric Models (PCLSAM) (Chou et al., 1999) algorithm. While kCARTA was developed for use in the infrared region ($605\text{-}2830\text{ cm}^{-1}$), it is trivial to extend the database out in either direction, to span the Far InfraRed to the Ultra-Violet. A clear-sky only radiance+jacobian Matlab version is also available.

65 The speed and accuracy, plus available run-time options of the code make it a very attractive alternative to other existing line by line codes. The literature is replete with papers and books describing spectroscopic calculations, monochromatic radiative transfer and flux calculations (see for example (Goody and Yung, 1989; Edwards, 1992; Clough et al., 1992; Clough and Iacono, 1995; Tjemkes et al., 2002; Buehler et al., 2011; Schreier et al., 2014; Dudhia, 2017; Vincent and Dudhia, 2017)) so here we chose to emphasize the features (and limitations) of kCARTA that would interest researchers working in these and related
70 fields, and apply kCARTA to quantify how different spectroscopic databases impact simulated clear-sky Top of Atmosphere (TOA) brightness temperatures. Focusing on the infrared ($605\text{ - }2830\text{ cm}^{-1}$) region, this paper begins with a description of the line-by-line code and the kCompressed database, followed by a description of the clear sky radiative transfer algorithm, together with jacobians. The paper then discusses in detail some of the internal machinery of kCARTA, such as a background thermal computation developed for kCARTA, flux computations and scattering packages.

75 2 Overview of line-by-line code and kCompressed Database

2.1 UMBC-LBL

For an input set of [average temperature, pressure and gas amount (in molecules/cm²)] parameters, a custom monochromatic line-by-line code (UMBC-LBL) (De Souza-Machado et al., 2002) has been developed in order to accurately compute optical depths. This code defaults to the Van Vleck and Huber lineshape (Van Vleck and Huber, 1977; Clough et al., 1980) for almost
80 all molecules, using spectroscopic line parameters from the High-resolution TRANsmission (HITRAN) molecular absorption database.

For each spectral region the UMBC-LBL optical depth computations are divided into bins that are typically 1 cm^{-1} wide in the infrared. The optical depth in each of these bins is accumulated in three stages as shown in Figure 1 : (1) fine mesh stage - absorption due to line centers within 1 cm^{-1} of the bin edges is included at a very high resolution (typically 0.0005 cm^{-1})
85 and then five point boxcar integrated to the output (typically 0.0025 cm^{-1}) grid; in Figure 1 these are the red lines within the bin edges at $\pm 0.5\text{ cm}^{-1}$ and the blue lines within 1 cm^{-1} of the same bin edges (2) medium mesh stage - absorption from line centers within $1\text{-}2\text{ cm}^{-1}$ of the bin edges is included at 0.1 cm^{-1} resolution, shown in green in the figure and finally (3) coarse mesh stage - absorption from line centers within $2\text{-}25\text{ cm}^{-1}$ of the bin edges, are included at 0.5 cm^{-1} resolution (none shown)

in the figure); for (2) and (3) the results are interpolated to the output ~~0.0025~~-grid. The black line is the accumulated optical depth for that bin.

We note ~~two-three~~ points here. First, the ~~above-default~~ kCARTA uses 0.0005 cm⁻¹ resolution between 605-880 cm⁻¹ and 0.0025 cm⁻¹ from 805-2830 cm⁻¹ (after the 5 point boxcar). Section 7 demonstrates convolved radiances computed with these resolutions compare very well against other RTAs, especially after convolving with a typical hyperspectral sounder response function. Second, the above line-by-line computations are very similar to those in other models (Edwards, 1992; Dudhia, 2017), but we use the “medium” bins and “coarse” bins for the lines whose centers are within the intervals lying $\pm [1,2]$ and $\pm [2,25]$ cm⁻¹ respectively of the bin edges, instead of using only “coarse” bins. ~~Second,~~ Thirdly we note that for most Earth atmosphere molecules, the line strength \times gas amount combination means the optical depth contribution due to line centers further than 25 cm⁻¹ away from the bin is negligible and can be ignored (Dudhia, 2017); the exception for the Earth atmosphere are H₂O and CO₂ which have countless strong lines further than 25 cm⁻¹ away from bin edges. To speed up the optical depth calculations, the weak but non-negligible contribution from these “far lines” is added in using a continuum optical depth contribution which depends on temperature and gas absorber amount.

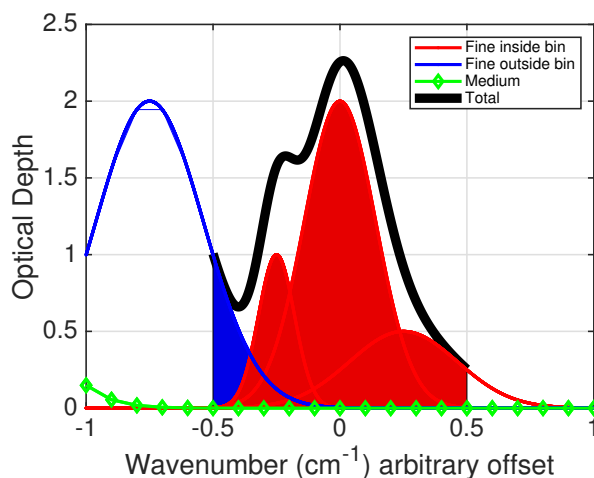


Figure 1. Line-by-line calculations from UMBC-LBL. The bin of interest is at $(-0.5,+0.5)$ cm⁻¹. Lineshapes whose line centers are within this bin (red) and within ± 1 cm⁻¹ of the bin edge (blue) are computed using high spectral resolution; line centers that are further out (green) have the lineshapes computed at medium resolution and then interpolated to a higher resolution; line centers even further away (not shown) are computed at coarse resolution. The black curve is the sum over all the line contributions within that bin.

The above steps are followed for almost all molecules. Modifications to the above steps are needed for water vapor (which is separated into the traditional "basement" plus "continuum" contributions (Clough et al., 1980, 1989)) and CO₂ in the 4 and 15 μ m region which needs line-mixing lineshapes (Strow and Pine, 1988; Tobin et al., 1996; Niro et al., 2005; Lamouroux et al., 2015). Other molecules have optical depths that are more easily modeled with the Van Huber lineshape, though recently the infrared absorption due to CH₄ has been modeled using line mixing (Tran et al., 2006). The UMBC-LBL optical depth

computation for water vapor should be robust at all frequencies, and allows the addition of water continuum models such as the recent MT-CKD 3.2 coefficients (Mlawer et al., 2012). Spectra from UMBC-LBL have been extensively compared against optical depths computed by models such as Line-by-line Radiative Transfer Model (LBLRTM) (Clough et al., 1992, 2005) and the General line-by-line Atmospheric Transmittance and Radiance model (GENLN2) (Edwards, 1992). ~~For example the optical depths of in the 10 region more closely resemble the reference monochromatic code MonoRTM than the code, which uses an accelerated algorithm for calculating the Voigt function (Mlawer, 2016).~~

2.2 kCompressed database

When applied toward any realistic Earth atmosphere simulation for an observing instrument, the UMBC-LBL calculations described above become impractically slow as they need to be performed for multiple gases in the atmosphere, over ~ 100 atmospheric layers and encompassing a wide spectral range.

UMBC-LBL is therefore primarily used to generate an uncompressed database of look-up tables as described below. For each gas other than water vapor, the spectra are computed using the US Standard Atmosphere temperature profile, as well as five temperature offsets (in steps of 10K) on either side of the temperature profile, for a total of 11 temperatures. Tests using NWP profiles show this is usually sufficient everywhere except for a handful over the winter Antarctica, which could fall slightly outside the coldest offset (on average by about 3 K) between 600-1000 mb; kCARTAhandles these extreme cold cases by extrapolating what has been compressed and zero checking the optical depths.

The default infrared database spans ~~605-605-880~~ 605-880 cm^{-1} ~~to 2830~~ and 805-2830 cm^{-1} , broken up into 10000 point intervals that are 5 cm^{-1} and 25 cm^{-1} wide respectively. Each file ~~contain~~ contains matrices to compute optical depths for these 10000 points at 0.0025 point spacing the set resolution. The one hundred average pressure layers used in making the database are from the AIRS Fast Forward Model. The layers span 1100 mb to 0.005 mb (about ground level to 85 km), and were chosen such that there is less than 0.1 K Brightness Temperature (BT) errors in the simulated AIRS radiances. The layers are about 200 m thick at the bottom of the atmosphere, gradually getting thicker with height (about 0.65 km at 10 km and 6 km at an altitude of 80 km).

These $10000 \times 100 \times 11$ optical depths intervals are then compressed using Singular Value Decomposition (SVD) to produce the kCompressed Database. Each compressed file will have a matrix of basis vectors B (size $10000 \times N$), and compressed optical depths D' (size $N \times 100 \times 11$), where N is the number of significant singular vectors found. The prime denotes the compression worked more efficiently when the optical depths were scaled to the $(1/4)$ power (Strow et al., 1998; Rodgers, 2000).

The self broadening of water is accounted for by generating monochromatic lookup tables for the reference water amount, multiplied by 0.1, 1.0, 3.3, 6.7 and 10.0 at the eleven temperature profiles specified above, meaning D' for water will have an extra dimension of length 5. Note that for the infrared we treat the HDO isotope (HITRAN isotope 4) as a separate gas from the rest of the water vapor isotopes.

The compressed optical depths D' vary smoothly in pressure, meaning the user is not limited to only using the 100 AIRS layers. For an arbitrary pressure layering, the look-up tables are uncompressed using spline or linear interpolation in temperature

and pressure, and scaled in gas absorber amount. Temperature interpolation of matrix D' for an AIRS 100 layer atmosphere therefore results in a matrix D'' of size $N \times 100$, and the final optical depths (of size 10000×100) are computed using $(BD'')^4$. Both the spline and linear interpolations allow easy computation of the analytic temperature derivatives, from which kCARTA can rapidly compute analytic ~~Jacobians~~ Jacobians (see Section 5). The cumulative optical depth for each layer in the atmosphere is obtained by a weighted sum of the individual gas optical depths, with accuracy limited by that of the compressed database (Strow et al., 1998). The interested reader is referred to (Vincent and Dudhia, 2017) for a further discussion of other RTAs that use compressed databases.

The most recent kCompressed database uses line parameters from the HITRAN 2016 database (Rothman et al., 2013; Gordon et al., 2017), which together with the UMBC-LBL lineshape models, determine the accuracy of the spectral optical depths in this database. UMBC-LBL CO₂ line-mixing calculations use parameters that were derived a few years ago. Newer line-mixing models exist and we now use optical depths computed using LBLRTM v12.8 together with the line parameter database file based on HITRAN 2012 (aer_v_3.6), and (a) CO₂ line mixing by (Lamouroux et al., 2010, 2015)) and (b) CH₄ line mixing by (Tran et al., 2006).

In addition complete kCompressed databases for the IR using optical depths only from HITRAN 2012, LBLRTM v12.4 code and from GEISA 2015 (Husson et al., 2015) have been generated for comparison purposes. At compile time we usually point kCARTA to the HITRAN 2016 kCompressed database made by UMBC-LBL, but at run time we have switches that easily allow us to swap in for example the CO₂ and CH₄ tables generated from LBLRTM.

The original lookup tables for the thermal infrared occupy hundreds of gigabytes, while the compressed monochromatic absorption coefficients are a much more manageable 824 megabytes (218 megabytes (water+HDO) + 76 megabytes (CO₂) + 530 megabytes (about 40 other molecular and 30 cross section gases)). A general overview of some of the factors involved in compressing look-up tables for use in speeding up line-by-line codes is found in (Vincent and Dudhia, 2017), while more details about the detailed testing and generation of the kCARTA SVD compressed database are found in (Strow et al., 1998). Appendix B discusses the extension of the database to span 15 cm^{-1} to 44000 cm^{-1} , though we note that kCARTA lacks built-in accurate scattering calculations in the shorter wavelengths. In order to resolve the narrow doppler lines at the top-of-atmosphere, the resolution $\delta\nu$ of the spectral ~~regions~~ bands in Appendix B is adjusted according to $\delta\nu \simeq \nu_0 \sqrt{(T/m)} \delta\nu \sim \nu_0 \sqrt{(k_b T/m)/c}$, where ν_0 is the band center, and T, m are the temperature and mass of the molecule respectively, while k_b and c are Boltzmann's constant and speed of light.

The default kCARTA mode is to use all the first 42 molecular gases in the HITRAN database, together with about 30 cross-section gases, for which we have reference profiles. If the user does not provide the profiles for any of these gases, kCARTA uses the US Standard profile for that gas. The user can also choose to only use a selected number of specified gases. While running kCARTA, the user can then define different sets of mixed paths, where some of the gases are either turned off or the entire profile is multiplied by a constant number, which is very useful when for example we want to include only certain gases when we parametrize optical depths for SARTA.

3 kCARTA Clear sky radiative transfer algorithm

175 As a stream of radiation propagates through a layer, the change in diffuse beam intensity $R(\nu)$ in a plane parallel medium is given by the standard [Schwartzschild-Schwarschild](#) equation (Liou, 1980; Goody and Yung, 1989; Edwards, 1992)

$$\mu \frac{dR(\nu)}{dk_e} = -R(\nu) + J(\nu) \quad (1)$$

where μ is the cosine of the viewing angle, k_e is the extinction optical depth, ν is the wavenumber and $J(\nu)$ is the source function. For a non-scattering “clear sky”, the source function is usually the Planck emission $B(\nu, T)$ at the layer temperature T , leading to an equation that can easily be solved for an individual layer. The general solution for a downlooking instrument measuring [radiating propagating radiation propagating](#) up through a clear-sky atmosphere can be written in terms of four components :

$$R(\nu) = R_s(\nu) + R_{lay}(\nu) + R_{th}(\nu) + R_{solar}(\nu) \quad (2)$$

185 which are the surface, layer emissions, downward thermal and solar terms respectively. In terms of integrals the expressions can be written as (see e.g. (Liou, 1980; Dudhia, 2017))

$$\begin{aligned} R(\nu, \theta) = & \epsilon_s(\nu) B(\nu, T_s) \tau_{atm}(\nu, \theta) + \int_{surface}^{TOA} B(\nu, T(z)) \frac{\partial \tau(\nu, \theta)}{\partial s} ds + \\ & \frac{1 - \epsilon_s(\nu)}{\pi} \tau_{atm}(\nu) \int d\Omega^+ \int_{TOA}^{surface} B(\nu, T(s)) \frac{\partial \tau(\Omega)}{\partial s} \cos(\theta) ds + \\ & \rho_s(\nu) B_{\odot}(\nu) \cos(\theta_{\odot}) \tau_{atm}(\nu, \theta_{\odot}) \tau_{atm}(\nu, \theta) \end{aligned} \quad (3)$$

190 where $B(\nu, T)$ is the Planck radiance at temperature T , T_s is the skin surface temperature, ϵ_s, ρ_s are the surface emissivity and reflectivity; $B_{\odot}(\nu)$ is the solar radiance at TOA, θ_{\odot} is the solar zenith angle; θ is the satellite viewing angle, $\tau(\nu, \theta)$ is the transmission at angle θ while τ_{atm} is the total atmospheric transmission. [The \$d\Omega^+\$ in the middle term indicates integration over the upper hemisphere.](#)

195 In what follows we discretize Eqn. 2 so that layer $i = 1$ is the bottom and $i = N$ ($=100$) the uppermost, schematically shown in Figure 2 for a clear sky four layer atmosphere, with O being the center of the Earth. A is the satellite while S is the satellite sub-point directly below it. Point P is the ground scene being observed by the satellite (slightly away from nadir), and N is the local normal at P . $\angle SAP$ is the satellite scan angle while $\angle APN$ is the satellite zenith angle θ ; $\angle NPI$ is the solar zenith angle θ_{\odot} . Note that as the radiation propagates through the pressure layers from P to H_1 to H_2 to H_3 to H_4 to A , the local angle (between the radiation ray and the local normal at any of the concentric circles) keeps changing due to the spherical geometry of the layers (refraction effects can also be included).

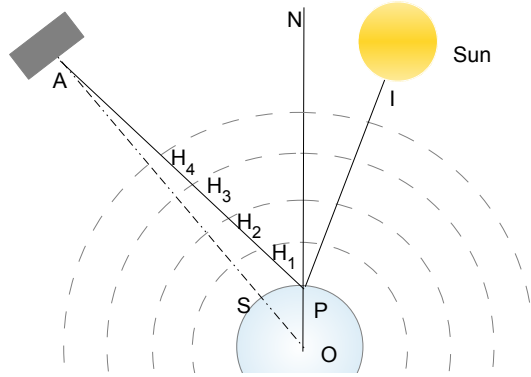


Figure 2. Viewing geometry for the sounders modeled by kCARTA. A is the satellite and point P is being observed by the satellite, while I is the sun

200 The default mode of kCARTA ~~assumes no~~ (f90) assumes linear variation of layer temperature with optical depth, uses a background thermal diffusive angle that varies with the layer-to-ground optical depth (instead of a constant value typically assumed to be $\cos^{-1}(3/5)$) and does ray-tracing to account for the spherical atmospheric layers (but with no density effects). The f90 version of kCARTA ~~allows the layer temperature to vary linearly with optical depth~~ also allows the user to choose constant layer temperature, and to choose alternate ways of computing the background term, which will be discussed in Section

205 6. ~~The individual~~

Here we describe radiative transfer for the constant layer temperature case; see Section 6.2 for a short discussion when using the linear-in-tau option. For an arbitrary layer i with (nadir) optical depth $k_i(\nu)$, the transmittance of a beam passing from the bottom to the top of the layer at angle θ is given by $\tau_i(\nu, \theta) = e^{-k_i(\nu)/\cos(\theta)}$. The transmittance from the top of layer i to space is then the product of the individual transmittances of the layers above i

$$210 \quad \tau_{i+1 \rightarrow TOA}(\nu, \theta) = \prod_{j=i+1}^N \tau_j(\nu, \theta) \quad (4)$$

with the special case of transmission from ground to space ($i = 0$) involving all N layers.

The individual contributions to the upwelling radiance are then computed as follows.

3.1 Surface emission

~~requires the user to supply the spectrally-varying emissivity (and surface reflectance).~~ The kCARTA surface emission is given

215 by

$$R_s(\nu) = \epsilon_s(\nu) B(\nu, T_s) \tau_{1 \rightarrow N \text{ GND} \rightarrow TOA}(\nu, \theta) \quad (5)$$

where $\epsilon_s(\nu)$ is the user supplied emissivity.

3.2 Layer emission

The atmospheric absorption and re-emission is modeled as :

$$220 \quad R_{\text{lay}} = \sum_{i=1}^{i=N} B(\nu, T_i) (1.0 - \tau_i(\nu)) \tau_{i+1 \rightarrow N} \tau_{i+1 \rightarrow \text{TOA}}(\nu, \theta) \quad (6)$$

Layers with negligible absorption ($\tau_i \rightarrow 1$) contribute negligibly to the overall radiance, while those with large optical depths ($\tau_i \rightarrow 0$) “black” out radiation from below. $(1.0 - \tau_i(\nu))$ is the emissivity of the layer while $(1.0 - \tau_i(\nu)) \tau_{i+1 \rightarrow N}(\nu, \theta)$ $(1.0 - \tau_i(\nu)) \tau_{i+1 \rightarrow \text{TOA}}(\nu, \theta)$ is the weighting function W_i of the layer.

3.3 Solar radiation

225 ~~Letting the surface reflectance be denoted by $\rho_s(\nu, \theta, \phi)$, then the solar contribution to the TOA radiance is given by-~~

$$\underline{R_{\odot}(\nu) \equiv \rho_s(\nu, \theta, \phi) B_{\odot}(\nu) \cos(\theta_{\odot}) \times \tau_{N \rightarrow \text{ground}}(\nu, \theta_{\odot}) \tau_{\text{ground} \rightarrow N}(\nu, \theta) \Omega_{\odot}}$$

~~Over ocean, if the wind speed and solar and satellite azimuth angles are known, the reflectance can be pre-computed using the Bi-directional Reflectance Distribution Function (BRDF) and input to ; see for example Appendix C in (Nalli et al., 2016). It is not easy to compute the BRDF over land, and the reflectance could be simply modeled as $\rho_s(\nu) = \frac{1 - \epsilon_s(\nu)}{\pi}$.~~

230 ~~$\Omega_{\odot} = \pi (r_s/d_{se})^2$ is the solid angle subtended at the earth by the sun, where r_s is the radius of the sun and d_{se} is the earth-sun distance. The solar radiation incident at the TOA $B_{\odot}(\nu)$ comes from data files related to the ATMOS mission (Farmer et al., 1987; Farmer and Norton, 1989), and is modulated by the angle the sun makes with the vertical, $\cos(\theta_{\odot})$ (day-of-year effects are not included in the earth-sun distance).~~

3.3 Background thermal radiation

235 The atmosphere also emits radiation downward, *at all angles*, in a manner analogous to the upward layer emission just discussed. The total background thermal radiance at the surface is an integral over all (zenith and azimuth) radiance streams propagating from the top-of-atmosphere (set to 2.7 K) to surface. This is time consuming to compute using quadrature, and one approximation is to use a single effective (or diffusivity) angle of $\theta_{diff} = \cos^{-1}(3/5)$ at all layers and wavenumbers :

$$R_{th}^{surface}(\nu) = \pi \rho_s \sum_{i=N}^{i=1} B(T_i) [\tau_{i-1 \rightarrow \text{ground}}(\nu, \theta_{diff}) - \tau_{i \rightarrow \text{ground}}(\nu, \theta_{diff})] \quad (7)$$

240 The summation is from top-of-atmosphere to ground, and ρ_s is the surface ~~reflectance~~ reflectivity discussed above. Current sounders have channel radiance accuracy better than 0.2K, so while the above term is much smaller than the surface or upwelling atmospheric emission contributions, it has to be computed accurately. Section 6 includes a detailed discussion of how kCARTA improves the accuracy of this background term by using a look-up table to rapidly compute a spectrally and layer varying diffusive angle.

245 4 Impact of spectroscopy on TOA BTs

3.1 Solar radiation

In this section is used to evaluate how spectroscopy impacts the simulated BTs at the TOA. First we evaluate differences between spectral databases (2012, 2016 and 2015), and then we assess how spectroscopic line parameter uncertainties impact the BTs. The satellite scan angle in all calculations is 22, which is about half the maximum scan of the AIRS, CrIS and IASI
250 sounders. Letting the surface reflectivity be denoted by $\rho_s(\nu, \theta, \phi)$, then the solar contribution to the TOA radiance is given by

3.2 Top of Atmosphere BTs computed using different databases

$$\underline{R_{\odot}(\nu)} \equiv \underline{\rho_s(\nu, \theta, \phi) B_{\odot}(\nu) \cos(\theta_{\odot}) \times \tau_{N \rightarrow \text{ground}}(\nu, \theta_{\odot}) \tau_{\text{ground} \rightarrow \text{TOA}}(\nu, \theta) \Omega_{\odot}} \quad (8)$$

For this section three spectral databases were used to compute TOA radiances (converted to BT) using . A set of 49 regression profiles typically expected in the Earth atmosphere (Strow et al., 2003) were used throughout this paper for this
255 and other studies. The profiles in this set include the US Standard temperature, pressure, and trace gas constituent fields (McClatchey et al., 1972), as well as the Mid-Latitude Summer/Winter, Polar Summer/Winter, Tropical profiles, and a set of extreme and intermediate hot/cold/dry/humid profiles chosen from the Thermodynamic Initial-Guess Retrieval (TIGR) database (Achard, 1991) to span the expected variability of profiles in the Earth's atmosphere (Strow et al., 2003). The results are shown in Figure ??.

260 For the left panels (a) three databases were used : (1) default 2016 (2) 2012 and (3) GEISA 2015; all three used ,limemixing from v12.8 and we set to zero all optical depths from cross-section gases. For clarity we show results for a simulated AIRS instrument by convolving the computed monochromatic radiances using the AIRS Spectral Response Functions; the gaps in the plots are where AIRS has no detectors. This exercise is purely to show differences in the spectroscopy manifesting as equivalent BT differences, with validation against actual clear-sky observations left for a future paper. Panel (a) of Figure ?? show the
265 mean (top) and standard deviation (bottom) of the differences between HITRAN 2016 and 2015 (blue), HITRAN 2012 (red); the black curves are the AIRS NeDT. The obvious spectral differences are in the regions of the lines, especially in the 6.7 region; there are also noticeable differences in the HITRAN 2012-10 ; differences are also seen in the 2400–2700 region. These spectral differences are to be expected from the slightly differing spectroscopy in the individual databases; the interested reader who wishes to more completely fully interpret them is referred to the papers describing these individual databases.

270 The right panels (b) of Figure ?? shows the mean (top) and standard deviation (bottom) of the differences between the spectroscopy between default LBLRTM v12.8 and two other databases : (1) (blue) and (2) LBLRTMv12.4 (red). The black curves in the top panel are the column jacobian for a ± 5 ppm change, and shows the differences in the LBLRTM versions are within that amount; the bottom sagain shows the standard deviation of the differences. The differences compared to the older line mixing model (which was developed using 2000 line parameters) is much larger in the 690-720 region. A perusal of the
275 2000 where $B_{\odot}(\nu)$ is the solar radiation at the top of atmosphere and 2012 line parameters for the main isotope shows the main updates to the spectroscopy are to the air-accounts for the solar disk. Over ocean, if the wind speed and solar and satellite

azimuth angles are known, the reflectivity can be pre-computed using the Bi-directional Reflectance Distribution Function (BRDF) and self-broadening linewidth coefficients in input to kCARTA; see for example Appendix C in (Nalli et al., 2016). It is not easy to compute the BRDF over land, and the 600-730 range, which would impact the line mixing relaxation matrices.

280 We note the model currently in use for AIRS L2 retrievals was developed in 2010 and has been tuned against observations; a more updated model using HITRAN 2016 line parameters together with LBLRTM 12.8, line mixing spectroscopy is currently being developed. reflectivity could be simply modeled as $\rho_s(\nu) = \frac{1 - \epsilon_s(\nu)}{\pi}$.

Comparing different spectroscopic databases, with top/bottom panels showing the mean and standard deviation over 49 regression profiles. Left panel (a): H2016 versus 2015 (blue) and H2012 (red). The black curve is the AIRS NeDT. Right panel 285 (b): 15 CO2 line mixing differences, compared to LBLRTM 12.4 (red) and (blue). For both sets of plots the top is the mean differences versus the control (HITRAN 2016 with line mixing from LBLRTM v12.8, evaluated over our 49 regression profile set

3.2 Impact of spectroscopy error budget on Top of Atmosphere BT

The and databases are bundled with error indices associated with the individual spectroscopic line parameters. The uncertainty 290 codes in the database (Rothman et al., 2005) are replicated in Table ?? for convenience. As seen from the table, the uncertainties are divided into two groups: absolute (wavenumber and pressure shift) and relative (intensity and broadening parameters).

Wavenumber and Intensity, Halfwidths, and Pressure shift (cm-1) Temperature-dependence Code Uncertainty Range Code
Uncertainty Range 0 ≥ 1 . or Unreported 0 Unreported or Unavailable 1 ≥ 0.1 and < 1 . 1 Default or Constant 2 ≥ 0.01 and < 0.1 2 Average or Estimate 3 ≥ 0.001 and < 0.01 3 $\geq 20\%$ 4 ≥ 0.0001 and < 0.001 4 $\geq 10\%$ and $< 20\%$ 5 ≥ 0.00001 and < 0.0001 5 $\geq 5\%$ and $< 10\%$ 6 ≥ 0.000001 and < 0.00001 6 $\geq 2\%$ and $< 5\%$ 7 ≥ 0.0000001 and < 0.000001 7 $\geq 1\%$ and $< 2\%$ 8 ≥ 0.00000001 and < 0.0000001 8 $< 1\%$ 9 \geq Better than 0.00000001 Meaning of HITRAN uncertainty codes

It is relatively straightforward to use these indices to include the associated uncertainty of any relevant line parameter for most gases, and generate a new compressed database using . Exceptions arise because the HITRAN 1986 database edition did not have uncertainties and was populated with zeros, a few of which have not yet been updated (Gordon, 2018). In these cases 300 the uncertainty index is 0 (for the left column of the table) or 0,1,2,3 (for the right part of the table). The value of 0 occurs for example, in many of the line strength uncertainties for the 10 isotopes 1,2; to remedy this we used 3% which is slightly lower than the 4% estimated in (Drouin et al., 2017; Birk et al., 2019). Similarly many of the strong 7.6 lines (isotope 1) are assigned an intensity uncertainty code of 3; to our knowledge there is no other additional information and we used a maximum value of 20% (Gordon, 2018). We also used 0.1, 0.1/atm uncertainties for the line center and pressure shift when the uncertainty index 305 was 0 (Gordon, 2018).

In Figures ?? and ?? below, we concentrate on the changes in computed BT effects after we perturb individual parameters for the first few molecules in the HITRAN database (,,,). The red curves in the top and bottom panels show mean and standard deviations of the $\Delta(BT)$ averaged over 49 regression profiles. The black curve are the AIRS NeDT at 250 K. We avoid perturbing , as it would involve coupling to the line mixing code (with its associated parametrized continuum); to a certain

310 extent the right hand panel of Figure ?? alleviates this omission as it compares different linemixing models. We used the Van
Huber lineshape for to avoid these same line-mixing complexities.

$\Delta(BT)$ for perturbations to (a) strength and (b) broadening parameters. The top and bottom panels show mean and standard
deviations of the changes, while the black curves are the AIRS NeDT at 250 K. Many of the line uncertainties (near the 1305
region) were set at 20% because of the lack of information for those lines.

315 $\Delta(BT)$ for perturbations to (a) wavenumber and (b) line shift due to pressure parameters. The top and bottom panels show
mean and standard deviations of the changes, while the black curves are the AIRS NeDT at 250 K. Most of the perturbations
were below the 0.1 level.

The perturbed parameters are line strength and all the broadening parameters (Figure ??), and wavenumber and line center
shift due to pressure (Figure ??). These figures show that the uncertainty in the HITRAN line parameters are typically less
320 than the noise of the current generation of sounding instruments; the reality is $\Omega_{\odot} = \pi(r_s/d_{se})^2$ is the biggest problems are
older and strengths and broadening uncertainty indices that need to be updated (Gordon, 2018). A similar calculation where
we assumed the uncertainties were independent of each other allowed us to randomize all perturbations to be within 0 and $\pm X$
(where X solid angle subtended at the earth by the sun, where r_e is the radius of the sun and d_{se} is the maximum number
corresponding to the error indices in Table ??); this roughly halves the largest errors shown in these two figures, so they are
325 within ± 1 K in the region earth-sun distance. The solar radiation incident at the TOA $B_{\odot}(\nu)$ comes from data files related
to the ATMOS mission (Farmer et al., 1987; Farmer and Norton, 1989), and is modulated by the angle the sun makes with the
vertical, $\cos(\theta_{\odot})$ (day-of-year effects are not included in the earth-sun distance).

4 Non Local Thermodynamic Equilibrium computations

During the daytime, incident solar radiation is preferentially absorbed by some CO₂ and O₃ infrared bands, whose kinetic
330 temperature then differs from the rest of the bands or molecules. This leads to enhanced emission by the lines in these bands.

Limb sounders detect NLTE effects in the 15 μm CO₂ bands (and in other molecular bands for example O₃) due to the
extremely long paths involved, but these are not modeled in the package as kCARTA is designed for nadir sounders.

For a nadir sounder, the most important effects are seen in the CO₂ 4 μm (ν_3) band. kCARTA includes a computationally
intensive line-by-line Non Local Thermodynamic Equilibrium (NLTE) model to calculate the effects for this CO₂ band. The
335 model requires the kinetic temperature profile and NLTE vibrational temperatures of the strong bands in this region, to compute
the optical depths and Planck modifiers for the strong NLTE bands and the weaker LTE bands (Edwards et al., 1993, 1998;
Lopez-Puertas and Taylor, 2001; Zorn et al., 2002), which are then used to compute a monochromatic top-of-atmosphere nadir
radiance.

AIRS provided the first high resolution nadir data of NLTE in the 4 micron CO₂ band. Using the kCARTA NLTE line-by-line
340 model, a Fast NLTE Model (De Souza-Machado et al., 2007) for sounders has already been developed, which is used in the
NASA AIRS L2 operational product.

5 Clear Sky Jacobian algorithm

Retrievals of atmospheric profiles (temperature, humidity and trace gases) minimize the differences between observations and calculations, by adjusting the profiles using the linear derivatives (or jacobians) of the radiance with respect to the atmospheric parameters. This section describes the computation of analytic jacobians by kCARTA. Note that kCARTA currently computes jacobians and weighting functions using a constant layer temperature assumption. For a downward looking instrument, for simplicity consider only the upwelling terms in the radiance equation (atmospheric layer emission and the surface terms). Assuming a nadir satellite viewing angle, the solution to Equation 1 is :

$$R(\nu) = \epsilon_s B(T_s, \nu) \tau_{1 \rightarrow N, 1 \rightarrow TOA}(\nu) + \sum_{i=1}^{i=N} B(T_i, \nu) (1.0 - \tau_i(\nu)) \tau_{i+1 \rightarrow N, i+1 \rightarrow TOA}(\nu) \quad (9)$$

350 Differentiation with respect to the m -layer variable s_m , (gas amount or layer temperature $s_m = q_{m(g)}, T_m$) yields

$$\frac{\partial R(\nu)}{\partial s_m} = \epsilon_s B(T_s) \frac{\partial \tau_{1 \rightarrow N}(\nu)}{\partial s_m} \frac{\partial \tau_{1 \rightarrow TOA}(\nu)}{\partial s_m} + \sum_{i=1}^N B(T_i, \nu) (1.0 - \tau_i(\nu)) \frac{\partial \tau_{i+1}(\nu)}{\partial s_m} + \sum_{i=1}^N \tau_{i+1 \rightarrow N, i+1 \rightarrow TOA}(\nu) \frac{\partial}{\partial s_m} [B(T_i, \nu) (1.0 - \tau_i(\nu))]$$

where as usual, $\tau_m(\nu) = e^{-k_m(\nu)}$, $\tau_{m \rightarrow N}(\nu) = \prod_{j=m}^N e^{-k_j(\nu)}$, $\tau_{m \rightarrow TOA}(\nu) = \prod_{j=m}^N e^{-k_j(\nu)}$. The differentiation yields

$$\begin{aligned} \frac{\partial R(\nu)}{\partial s_m} = & \left[\epsilon_s B(T_s) \tau_{1 \rightarrow N, 1 \rightarrow TOA} \right] (-1) \frac{\partial k_m(\nu)}{\partial s_m} + \\ & \left[\sum_{i=1}^{m-1} (1.0 - \tau_i(\nu)) B_i(\nu) \tau_{i+1 \rightarrow N, i+1 \rightarrow TOA} \right] (-1) \frac{\partial k_m(\nu)}{\partial s_m} + \\ 355 & \left[(1.0 - \tau_m(\nu)) \frac{\partial B_m(\nu)}{\partial s_m} - B(T_m, \nu) \frac{\partial \tau_m(\nu)}{\partial s_m} \right] \tau_{m+1 \rightarrow N, m+1 \rightarrow TOA}(\nu) \end{aligned} \quad (11)$$

The individual Jacobian-jacobian terms $\frac{\partial k_m}{\partial s_{m(g)}}$ are rapidly computed by kCARTA, as follows. The gas amount derivative is simply $\frac{\partial k_m}{\partial q_{m(g)}} = \frac{k_m}{q_{m(g)}}$ (with added complexity for water, to account for self broadening), and the temperature derivative $\frac{\partial k_m}{\partial T}$ is cumulatively obtained *while* kCARTA is performing the temperature interpolations during the individual gas database uncompression.

360 The solar and background thermal contributions are also included in the Jacobian-jacobian calculations. The thermal background Jacobians-jacobians are computed at $\cos^{-1}(3/5)$ at *all* levels, for speed. This would lead to slight differences when comparing the Jacobians-jacobians computed as above to those obtained using finite differences. The Jacobians-kCARTA also computes the weighting functions, and jacobians with respect to the surface temperature and surface emissivity are also computed, as are the weighting functions.

365 6 Background thermal and temperature variation in a layer

In this section we take a closer look at the computation of downwelling background thermal radiation, and layer temperature variation.

6.1 Background thermal radiation

The contribution of downwelling background thermal to top-of-atmosphere upwelling radiances is negligible in regions that
 370 are blacked out as the instrument cannot see surface leaving emission. Similarly in layers/spectral regions where there is very
 little absorption and re-emission, the contribution is negligible as the effective layer emissivity (denoted by $\Delta\tau_i(\nu)$ below)
 goes to zero. The background contribution thus needs to be done most accurately in the window regions (low but finite optical
 depths) ; depending on the surface ~~reflectance~~ emissivity (and hence reflectivity) in the window regions, in terms of BT this
 term ~~contribute~~ contributes as much as 4 K of the total radiance when reflected back up to the top of the atmosphere.

375 The contribution at the surface by a downwelling radiance stream propagating at angle (θ, ϕ) through layer i is given by

$$\begin{aligned}\Delta R_i(\nu, \theta, \phi) &= B(\nu, T_i)(1.0 - \tau_i(\nu, \theta, \phi))\tau_{i-1 \rightarrow \text{ground}}(\nu, \theta, \phi) \\ &= B(\nu, T_i)(\tau_{i-1 \rightarrow \text{ground}}(\nu, \theta, \phi) - \tau_{i \rightarrow \text{ground}}(\nu, \theta, \phi))\end{aligned}\quad (12)$$

where θ is the zenith and ϕ is the azimuth angle, and $\tau_{i \rightarrow \text{ground}}$ are the layer-to-ground transmittances, derived from layer-
 to-ground optical depths x . This equation can be rewritten as

$$380 \quad \Delta R_i(\nu, \theta, \phi) = B(\nu, T_i) \times \Delta\tau_i(\nu, \theta, \phi) \quad (13)$$

An integral over (θ, ϕ) would give the contribution from the layer. The total downwelling spectral radiance at the surface
 would be a sum over all i layers (and the downwelling flux at the surface would be the integral over all wavenumbers).

The integral over the azimuth is straightforward (assuming isotropic radiation), but the integral over the zenith is more
 complex. Since the reflected background term is much smaller than the surface or atmospheric terms, a single stream at the
 385 effective angle $\theta_{diff} = \cos^{-1}(3/5)$ (Liou, 1980) is often used as an approximation, at all layers and wavenumbers.

We have refined the computation as follows. Recall that $\Delta R(\nu)$ in Equation 13 depends on the layer-to-ground optical depth
 x . Letting $\mu = \cos\theta$ the integral over the zenith (~~$\int_0^1 \mu d\mu e^{-x/\mu} = E_3(x)$~~ $\int_0^1 e^{-x/\mu} \mu d\mu = E_3(x)$, more commonly known as the
exponential Integral of the third kind). The area under the $E_3(x)$ curve would be the total flux coming from all optical depths
 $(0 \leq x \leq \infty)$; over 77% of this area comes from the range $0 \leq x \leq 1$.

390 Applying the Mean Value Theorem for Integrals (MVTI) to $E_3(x)$, we can write Eq. 13 in terms of two effective diffusive
 angles $\theta_d^i, \theta_d^{i-1}$ at each layer i :

$$\begin{aligned}\Delta\tau(i, i-1) &= \tau(i-1 \rightarrow \text{ground}, \theta_d^{i-1}, \nu) - \tau(i \rightarrow \text{ground}, \theta_d^i, \nu) \\ R_{th}^{surface}(\nu) &= 2\pi\rho_s \sum_{i=N}^{i=1} B(\nu, T_i) \Delta\tau(i, i-1)\end{aligned}\quad (14)$$

with the effective angles varying as a function of the layer to ground space optical depth of that layer, and the layer immediately
 395 below it. Numerical solutions to the MVTI show that when $x \rightarrow 0$ then $\mu_d \rightarrow 0.5$ (or $\theta_d \rightarrow 60^\circ$). Similarly as $x \rightarrow \infty$ then

$\theta_d \rightarrow 0^\circ$, but this optically thick atmosphere means an instrument observing from the TOA cannot see the surface, so we use a lower limit (of 30°) for the diffusive angle. Finally when $x = 1.00$ we find the special case $\mu_d = 0.59274 \simeq (3/5)$. For “optically thin” regions, the layers closest to the ground contribute most to $R_{th}(\nu)$.

400 With today’s high speed computers, kCARTA uses an effective diffusive angle θ_d tabulated as a function of layer to ground optical depth x , as follows. For each 25 cm^{-1} interval spanning the ~~infrared~~infrared the layer L above which $\cos^{-1}(3/5)$ can be safely used was determined; below this layer, the lookup table is used. The table has higher resolution for $x \leq 0.1$ and becomes more coarse as x increases, with the effective diffusive angle cutoff at 30° when the optical depths are larger than about 15.

405 We have tested this method of computing the background thermal against both 20 point Gauss-Legendre quadrature and the 3 point exponential Gauss-quadrature (used by ~~LBLRTM~~LBLRTM flux computations), and found the method to very accurate and fast, both in terms of the downwelling flux at the surface, and also the final TOA computed radiance, even when the emissivity is as low as 0.8 (which means a significant contribution from the reflected thermal). At this low emissivity value, the constant ~~$\arccos(3/5)$~~ $\cos^{-1}(3/5)$ diffusivity angle model produces final TOA BT which differ from the Gauss-Legendre model by as much as 1.3 K (for the tropical profile) at for example 900 cm^{-1} , while the exponential quadrature and our model have errors smaller than 0.005 K.

410 6.2 Variation of layer temperature with optical depth

LBLRTM (Clough et al., 1992, 2005) has been extensively tested and shown to be very accurate, in its computation of optical depths, radiances and fluxes. In the computation of radiances, ~~the main difference between the both~~ both kCARTA and LBLRTM codes ~~is that for each spectral point, the former defaults to use~~ a “constant linear” in τ layer temperature ~~variation, while the latter uses a “linear in”~~; the former uses a higher order expansion (accurate to $O(\tau^5)$ for small τ layer temperature variation), and also has an option to use “constant” layer temperature. Here we summarize the relevant equations, ~~and briefly discuss the computed differences using~~. For an individual layer, with lower and upper boundary temperatures T_L, T_U , the “linear in τ ” approximation leads to the following expression for the radiance at the top of the layer (re-written from Equation 13 in (Clough et al., 1992))

$$I(\nu) = I_0(\nu)T + (1 - T) \left\{ B_{av}(\nu) + (B_u(\nu) - B_{av}(\nu)) \left(1 - 2 \left(\frac{1}{\tau} - \frac{T}{1 - T} \right) \right) \right\} \quad (15)$$

420 where the optical depth τ includes the view angle $\tau = \tau_{layer} / \cos(\theta)$ and transmission $T = \exp(-\tau)$. $I_0(\nu)$ is the radiation incident at the bottom of the layer, $B_{av}(\nu)$ is the Planck radiance corresponding to the average layer temperature, while $B_u(\nu)$ is the Planck radiance corresponding to the upper boundary. For large τ , $T \rightarrow 0$ and $I(\nu) \rightarrow B_u(\nu)$. For small $\tau \rightarrow 0$ the expression can be further expanded as follows

$$I(\nu) = I_0(\nu)T + (1 - T) \left\{ B_{av}(\nu) + (B_u(\nu) - B_{av}(\nu)) \left(\frac{\tau}{6} - \frac{\tau^3}{360} + \frac{\tau^5}{15120} \right) \right\} \quad (16)$$

425 Comparing to the top of layer radiance in the “constant in τ ” model,

$$I(\nu) = I_0(\nu)T + (1 - T)B_{av}(\nu) \quad (17)$$

one sees the expressions are identical if there is no temperature variation ~~ie i.e.~~ ($B_u(\nu) = B_{av}(\nu)$). The default kCARTA model layers are approximately 0.25 km thick (or a temperature spread of about 1.5 K for a 6K/km lapse rate) at the bottom of the atmosphere, and about 2 km thick in the stratosphere (a temperature difference of 10 K). ~~However the~~ The gaseous absorption in these upper layers is typically negligible, except deep inside the strongly absorbing 15 μm and 4 μm CO₂ bands. ~~Differences in BTs computed using the "constant" versus "linear" models will be expected to be greatest in these regions. The US Standard, Tropical, Mid Latitude and Polar Summer/Winter profiles were used to evaluate the differences between the "constant" versus "linear" models. The monochromatic results clearly showed the expected mean BTDs as large as 10 K or more in the optically thick (, which is where one would expect the largest differences between a linear-in-tau versus a constant-in-tau temperature model.~~

7 RTA inter-comparisons : kCARTA versus LBLRTM

In this section we describe brightness temperature differences (ΔBT) between kCARTA and LBLRTM. As kCARTA is designed to be accurate for typical hyperspectral sounders, we show that after convolution the kCARTA spectral radiances compare very well against similarly convolved LBLRTM radiances; for completeness we also discuss how the monochromatic (ΔBT) change as a function of resolution in the 10-15 μm O₃ and temperature sounding regions.

For these runs we use our 49 regression profiles, with emissivity = 1 and reflectivity = 0 to exclude differences due to reflected thermal contributions. To exercise the kCARTA ray tracing, we use a ground satellite zenith angle of 24.5° which becomes a TOA satellite scan angle of 22° (typical average sounder scan angle). The tests are run at various kCARTA database resolutions. Note that when results are stated for a particular resolution, this means the kCARTA database (after 5 point boxcar integration) was at this resolution; similarly the internal LBLRTM radiances were output at a resolution such that we can apply the same 5 point boxcar for the radiance comparisons.

The comparisons are divided into two sets. For the first set of comparisons, we use an atmosphere consisting only of H₂O, CO₂, O₃, with the optical depths generated using LBLRTM v12.8. This is done to assess the linear-in-tau radiative transfer while limiting differences due to spectroscopy, especially in the high altitude 15 μm CO₂ and 10 μm O₃ sounding regions. For these tests, three resolutions spanning 605-1205 cm⁻¹ were used : 0.0025 cm⁻¹, 0.0005 cm⁻¹ and 0.0002 cm⁻¹.

At low resolution (0.0025 cm⁻¹), the mean differences right on top of the high altitude temperature sounding lines in the 630-700 cm⁻¹ region are large (> 10 K). However, these differences drop significantly as we increase the resolution, to within 4)regions, and systematically much smaller in the window or regions dominated by and absorption. After convolving the computed radiances over the AIRS $K \pm 1.2$ K at 0.0005 cm⁻¹ (default kCARTA resolution) and 1 K ± 0.4 K at 0.0002 cm⁻¹. The default kCARTA 0.0005 cm⁻¹ resolution results are shown in the left hand panels (a),(b) of Figure 3. The top panel is the mean while the bottom panel is the standard deviation. Note that in the 10 μm O₃ sounding region (where the doppler

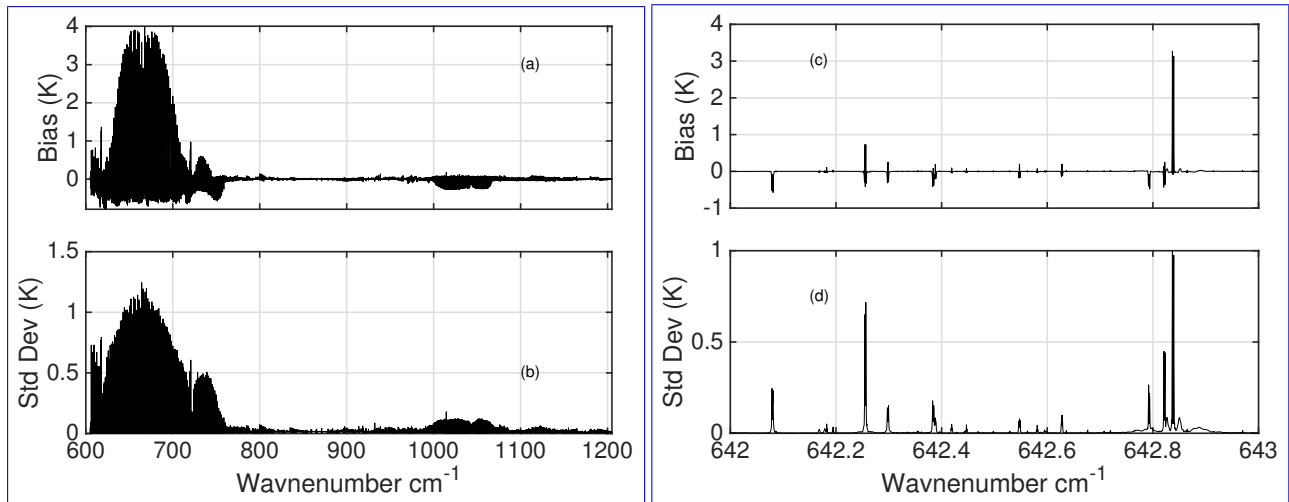


Figure 3. The top/bottom panels show the monochromatic BT differences (LBLRTM- kCARTA), with statistics obtained over 49 regression profiles, with the emissivity set to 1.0 and a 22° satellite scan angle. Both sets of panels shows the differences at 0.0005 cm⁻¹ resolution when only H₂O, CO₂ and O₃ optical depths from LBLRTMv12.8 are used. The largest differences are at the peaks of the high altitude 15 μm CO₂ lines, and decrease as the resolution is increased. The right hand panels are a zoom in of the left hand panels, for a typical 15 μm region.

broadened width of the high altitude lines would be wider than in the 15 μm region), the differences are consistently much smaller: -0.3 ± 0.1 K at 0.0005 cm⁻¹ resolution, dropping to -0.1 ± 0.05 K at 0.0002 cm⁻¹ resolution.

460 The right hand (c),(d) panels of Figure 3 are a zoom-in of a typical unit wavenumber interval deep in the 15 μm region, and shows the differences are zeros away from lines and largest around the peaks of the high sounding lines, each encompassing a very narrow spectral range of less than ~ 0.005 cm⁻¹. These would be expected to contribute minimally to the convolutions using typical sounder spectral response functions, the mean differences typically dropped to below 0.05 K in the opaque regions (except exactly at the peak of the dominant 667 as will be shown below).

465 Taken together these mean that the kCARTARTA is working as expected: in the very long wavelength 15 μm CO₂ region the differences reduce as we increase the spectral resolution while at 10 μm the differences remain quite small. We conjecture the remaining differences between kCARTA and LBLRTM are due to (a) algorithms: we use Equation 16 to fifth order while LBLRTM may use a Padé approximation and/or Equation 16 to first order; (b) there may be some very slight broadening effects right on top of the high altitude CO₂ lines that we have not captured when generating the compressed database.

470 For the second set of monochromatic tests, kCARTA and LBLRTM used 42 molecular gases and 13 cross section gases, using the current kCARTA default resolution of 0.0005 cm⁻¹ Q-branch where the mean difference was about 0.2 K) / 0.0025 cm⁻¹ for the spectral ranges 605-880 cm⁻¹ / 805-2830 cm⁻¹; the overlap region allows us to convolve the resulting radiances with AIRS Spectral Response Functions (SRFs). Note that we used the default optical depths for kCARTA (currently HITRAN 2016, except for CO₂ and CH₄ which come from LBLRTMv12.8), while the LBLRTMv12.8 line-file is based on HITRAN 2012. We only briefly summarize the monochromatic differences: deep in the 15 μm they are the same as the left hand panels of

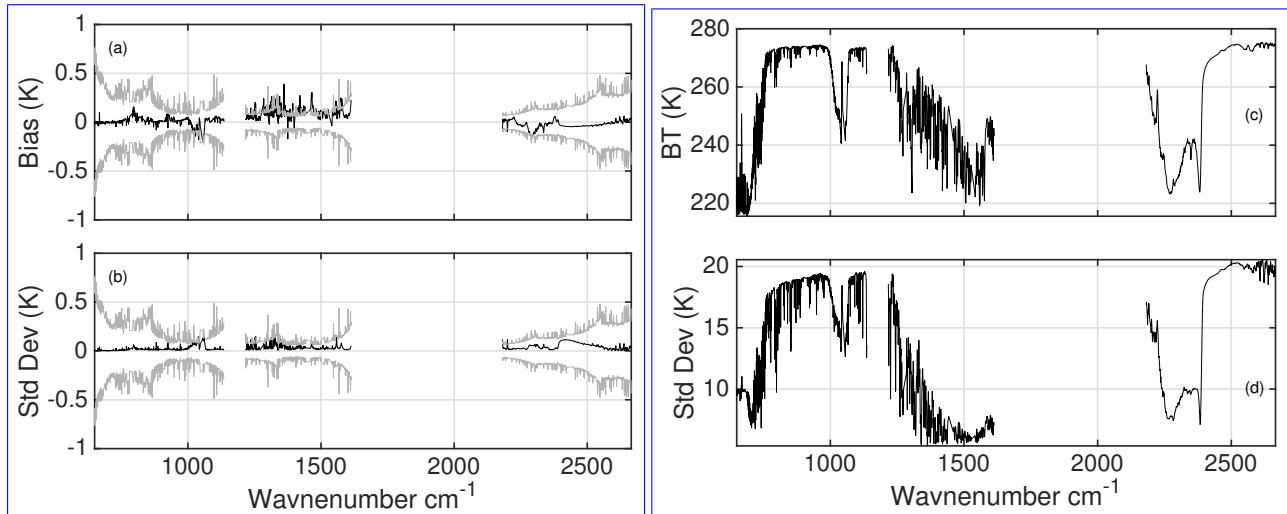


Figure 4. Results for 49 regression profiles, with 42 molecular gases and 13 cross section gases, convolved using AIRS SRFs. The emissivity was set to 1.0 and a 22° satellite scan angle. The left hand panels show the AIRS SRF convolved differences using the monochromatic differences (LBLRTM- kCARTA) seen in Figure 3, with the gray curves being the AIRS NeDT at 250 K, and are due primarily to the different spectroscopy used by the two RTAs (except for the CO₂ and CH₄ gases). The right hand panels show the mean calculated brightness temperature (top) and standard deviation (bottom). The variation in the 800-1200 cm⁻¹ region (and 2400-2680 cm⁻¹) is due to surface temperature differences and column water, while the variation in the other regions such as 10 μm and 7.6 μm is due to differing gas profiles of e.g. O₃ and H₂O; the variation in the 4 μm and 15 μm regions is due to temperature profile differences.

475 Figure 3, but are noticeably different in other regions because of differences in underlying spectroscopy and (for high altitude lines) possibly also resolution; for example on top of the 10 μm O₃ lines they could be as large as 5 K. Instead we show the differences after convolution with AIRS SRFs. The left hand panels (a),(b) of Figure 4 shows the biases and standard deviations of these differences; as described the noticeable differences at 10 μm and 6.7 μm arise primarily because of spectroscopy. For completeness, the right hand panels (c),(d) show the mean BT spectra for the 49 regression panels (top panel) and the variation in computed BT (bottom panel) which are due to profile differences (temperature, H₂O and O₃) as well as surface temperatures. Any user interested in reducing the monochromatic differences could easily do so by generating and using higher resolution compressed databases.

480

8 Flux Computations

Longwave fluxes at the top and bottom of the atmosphere, as well as the heating and cooling rates are computed by integrating spectral radiances from Equation 2 over all angles, and over the infrared spectral region : kCARTA is limited to the spectral range 15 - 3000 cm⁻¹ spanned by the different bands of kCARTA (see Appendix B). The major limitation of kCARTA for flux calculations is the fixed 0.0025-spectral (infrared) resolution at every layer, compared to the varying-with-

485

height resolution employed by other models such as LBLRTM. This impacts the high altitude longwave cooling in the 15 μm CO₂ band.

490 We use the Rapid Radiative Transfer ~~Model (RRTM-LW(Longwave) Model~~ (RRTM-LW) (Mlawer et al., 2012) as our reference model for flux and heating rate comparisons in a clear sky atmosphere. This fast model ~~compute~~ computes fluxes and heating rates in 16 bands spanning 10 cm⁻¹ to 3000 cm⁻¹, and was developed using LBLRTM; the latter uses a varying spectral resolution at each layer ($\delta\nu$ equal to 4 points per half-width in each layer) which means the spectra for the upper atmosphere layers have very high resolution. kCARTA uses the same approach as ~~RRTM~~ RRTM-LW and LBLRTM to compute
495 fluxes and heating rates : the angular integration uses an exponential Gauss-Legendre with 3 or 4 terms, with a "linear in τ " layer temperature variation.

The accuracy of the flux and heating rate algorithm in kCARTA at the ~~default 0.0025 resolution~~ various resolutions was assessed by comparing fluxes and heating rates in the dominant 15 μm to 10 μm bands (fourth to eighth ~~RRTM~~ RRTM-LW bands, spanning 630-1180 cm⁻¹) computed using ~~RRTM~~ RRTM-LW and kCARTA, using the 49 regression profile set.

500 At 0.0025 cm⁻¹ resolution the kCARTA and RRTM-LW heating rates differ by less than 0.2 K/day on average for altitudes below 40 km, but at higher altitudes the differences were much larger, and could be 1.5 K/day. ~~This was attributed to the default spectral resolution of in the 15 region. To test this, we generated a database of resolution 0.0005 spanning~~ Switching to the 605-1205 cm⁻¹ ~~for H₂O, CO₂ and O₃ which are by far the dominant absorbers in this spectral region, especially at higher altitudes. This significantly improved test atmosphere database at 0.0005~~ cm⁻¹ significantly improves the results, with heating
505 rate differences dropping to about 0.2 K/day almost everywhere.

Figure 5 shows the heating rate differences between kCARTA and ~~RRTM~~ RRTM-LW . The left panel shows differences between kCARTA and ~~RRTM~~ RRTM-LW , with the mean and standard deviation being solid and dashed respectively; the right panel shows mean calculations as a function of height. The blue curves were done at ~~default~~ 0.0025 cm⁻¹ resolution while the red curves were done at higher 0.0005 cm⁻¹ resolution. While the agreement is better than 0.05 K/day in the lowest 30 km,
510 Figure 5 shows the heating rates using the low resolution begin to differ noticeably above 45 km (blue curve); conversely the high resolution heating rates (red curves) are within 0.2 K/day till about 65 km.

~~Based on the above, users interested in flux calculations can improve the accuracy while retaining the speed advantages of by dividing the thermal infrared into two regions : 605-805 at 0.0005 resolution while the remaining 805-2830 region can have the current 0.0025 cm-1 resolution.~~

515 9 Scattering package included with f90 kCARTA

The daily coverage of hyperspectral sounders provides us with information pertaining to the effects of cloud contamination on measured radiances. Ignoring these effects can negatively impact retrievals used for weather forecasting and climate modeling. A scattering package based on the ~~PCLSAM~~ PCLSAM (Parametrization of Cloud Longwave Scattering for use in Atmospheric Models) scheme (Chou et al., 1999) has been interfaced into f90 kCARTA (see Appendix C). The implementation allows
520 kCARTA to compute radiances very quickly in the presence of scattering media such as clouds or aerosol. For a given scat-

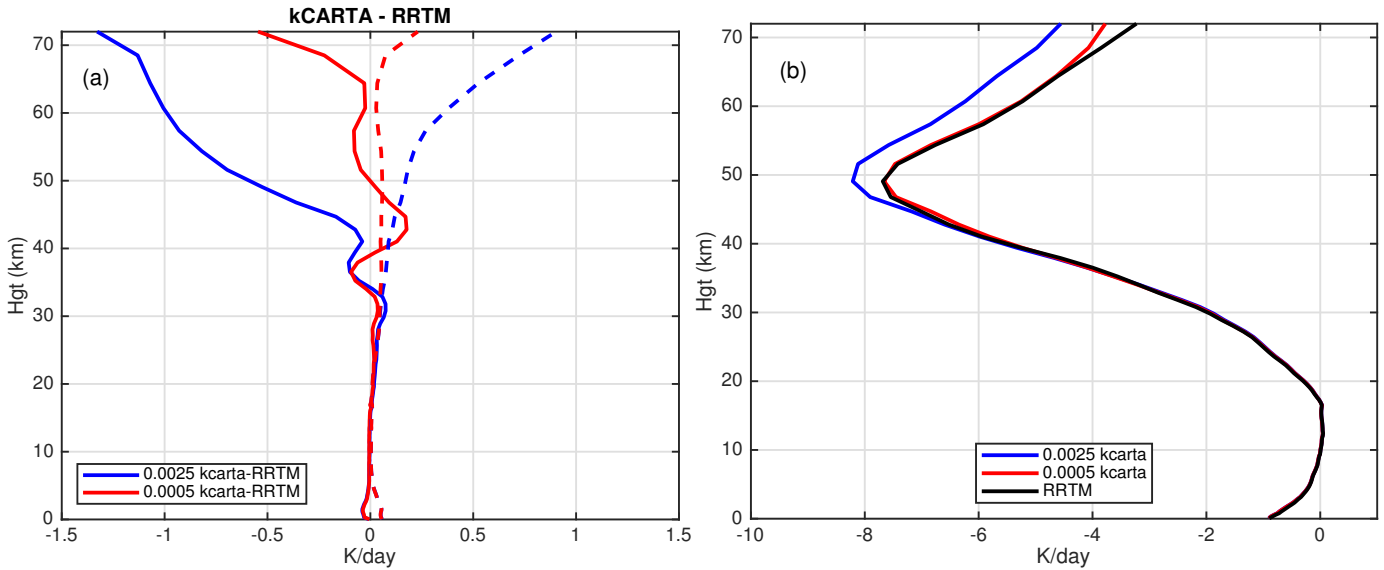


Figure 5. Heating rates for the $630\text{-}1180\text{ cm}^{-1}$ region computed using low (0.0025 cm^{-1} ; blue curves) and high (0.0005 cm^{-1} ; red curves) resolution kCARTA databases for 49 spanning Earth atmosphere profiles, compared to RRTM-LW. (a) The left panel shows differences in the heating rates, while (b) the right panel shows the mean heating rates.

tering species and assumed particle shape and distribution, the extinction coefficients, single scattering albedo and asymmetry parameters needed by the scattering code are stored in tables as a function of wavenumber and effective particle size (for a particle amount of 1 g/m^2). In addition The PCLSAM package is optimized for use in the thermal infrared, away from regions where solar contributions are important. As kCARTA currently does not handle e.g. Rayleigh scattering, one can easily use kCARTA to output monochromatic optical depths that can be imported into well known scattering packages. More details about PCLSAM PCLSAM and our cloud representation models are found in Appendix C.

10 Conclusions

We have described the details of a very fast and accurate pseudo- monochromatic code, optimized for the thermal infrared spectral region used by operational weather sounders for thermodynamic retrievals. It is much faster than line-by-line codes, and the accuracy of its spectroscopic database has been extensively compared against GENLN2 and more recently to LBLRTM. Updating the spectroscopy in a selected wavenumber region for a specified gas is as simple as updating the relevant file(s) in the database : for example, our custom UMBC-LBL enables us to re-build entire databases within weeks of the latest HITRAN release.

The computed clear sky radiances includes a fast, accurate estimate of the background thermal radiation. Analytic temperature and gas amount Jacobians-jacobians can be rapidly computed. Early in the AIRS mission, comparisons of AIRS observations against kCARTA simulations allowed for the quick implementation of modifications to gas optical depths : our

modifications to the CKD2.4 and MT-CKD 1.0 continuum versions are very similar to what is now in the MT-CKD2.5 version. We now use the MT-CKD 3.2 continuum, together with the N₂ and O₂ continuum contributions bundled with that same version. ~~The default infrared spectral resolution of~~ We use two resolutions in the infrared : 0.0005 cm⁻¹ for the 605-880 cm⁻¹ region ~~(to accurately resolve the high altitude CO₂ lines) and 0.0025 cm⁻¹ is good enough for nadir hyperspectral sounders; however at this resolution elsewhere; an user can easily switch to an alternate resolution by generating the appropriate compressed databases for use with kCARTA, though this could be at the expense of speed (at these current resolutions kCARTA has inaccuracies modeling fluxes in the takes 30 seconds to compute TOA spectra from 605-2830 cm⁻¹ while LBLRTM takes over three minutes). Tests show that brightness temperature differences between kCARTA and for example LBLRTM are largest right~~ on top of a small number of high altitude temperature sounding lines in the 15 μm band and radiances from limb sounders whose weighting function peak high in the atmosphere, though one can switch to a higher resolution database if needed.

~~We assessed how the uncertainties in the line parameters of the database impact top of atmosphere BTs for a nadir sounder, and found it typically is less than the NeDT of the current generation of sounders. The exceptions are and , but the remedy likely lies in correcting the uncertainty indices rather than the determination of the parameters themselves. In the future we plan to assess the line-mixing package supplied with the package, and plan to evaluate the impact of line parameter uncertainties on TOA BTs at that point region (and close to zero elsewhere); these differences reduce as the resolution is increased. Since the disparity is right at the peaks of the lines, the differences after convolution with a typical sounder SRF such as AIRS are on average much smaller than the NeDT.~~

kCARTA is fast enough to be used in Optimal Estimation retrievals for instruments spanning a reasonably small wavenumber range. The kCARTA database has been extended to include 15-44000 cm⁻¹, which eventually needs to be updated to HITRAN 2016 (see the Appendix). In the future we plan to augment the optical depth calculations performed by UMBC-LBL by using speed-dependent lineshapes as parameters become available.

Appendix A: Code availability

The UMBC-LBL code has been developed in Matlab, with extensive use of Mex files to speed up loops. The package is available at <https://github.com/sergio66/umbe-lbl-spectra> UMBC_LBL, and is fully described in (De Souza-Machado et al., 2002). The compression code is available upon request.

The f90 and Matlab versions of kCARTA can be cloned from https://github.com/sergio66/kcarta_gen and <https://github.com/strow/kcarta-matlab> respectively.

A1 UMBC-LBL and kCARTA downloads and auxiliary requirements

The kCompressed Database is supplied in Fortran little-endian binary files that contain the optical depths for a specific gas. Each file contains optical depths at 10000 spectral points × average pressures corresponding to the 100 AIRS layers. Links to the (605 - 2830 cm⁻¹) compressed database can be found at <http://asl.umbc.edu/pub/packages/kCompressedDatabase.html>

We also supply the US Standard Profile for all gases in the database, and ~~kLAYERS~~kLAYERS , a program that takes in a point profile (from sondes and NWP) and outputs an AIRS 100 layer path averaged profile (in molecules/cm²). ~~kLAYERS~~
570 ~~kLAYERS~~ needs our supplied HDF file implementation (RTP) source code.

The Matlab version should work with R2012+ while the compiler for the ~~fortran~~Fortran version must support structures, such as Absoft, ifort and PGF. As the RTP file contains the atmospheric profile and scan geometry, both the Matlab and f90 kCARTA only need a simple additional (namelist) file to drive either code. The f90 version of kCARTA outputs binary files, which typically have header information such as kCARTA version number, number of layers and gases and parameter setting
575 values, followed by panels, each 10000 points long, containing the optical depths, radiances, jacobians or fluxes computed and output by kCARTA. A number of Matlab based readers can then be used to further process the kCARTA output as needed. More information is found at <http://asl.umbc.edu/pub/packages/kcarta.html>.

[A new compressed database \(spanning the infrared 500-2830 cm⁻¹ region\) is generated for kCARTA every four years, roughly within a few months of a HITRAN database release. The current f90 version described in this paper is identified on github as SRCv1.21 f90 and currently uses HITRAN 2016 line parameters for all gases except CO₂ and CH₄ where we used LBLRTM v12.8 optical depths, together with MT-CKD3.2 continuum. These were used to generate the most recent SARTAv2.01 fast model coefficients; earlier SARTA versions were developed using kCARTAv1.07 and v1.18 \(with HITRAN databases updated as they became available\).](#)
580

Appendix B: Available spectral regions and f90 kCARTA features

585 The UMBC-LBL line-by-line code has been used to generate optical depths in the spectral regions seen in Table B1. The 605-2830 cm⁻¹ band is marked with an asterisk, since our work focuses on this spectral region. The current database in this spectral region uses lineshape parameters from HITRAN 2016. The Van Vleck and Huber lineshape is used for all HITRAN molecules from ozone ~~onwards~~onward; water vapor uses the “without basement” plus MT-CKD 3.2, and CO₂,CH₄ use line-mixing optical depths generated from ~~LBLRTM~~LBLRTM v12.8. Note that in the important 4.3 μm temperature sounding
590 region, the f90 version can also include the N₂/H₂O and N₂/CO₂ Collision Induced Absorption (CIA) effects modeled in (Hartmann et al., 2018; Tran et al., 2018), which depend on CO₂,H₂O and N₂ absorber amounts.

A clear-sky radiance calculation in the infrared takes about ~~20~~30 seconds, using a 2.8 GHz 32 core multi-threading Intel machine. The run-time goes to 120 seconds if ~~Jacobians~~jacobians are also computed (for 9 gases). A full radiance calculation from 15 to 44000 cm⁻¹ takes less than 5 minutes.

595 Table B2 lists a number of the features of kCARTA, with the ones marked by a asterisk only available in the f90 version. Note that the tables defaults to describing the spectroscopy for the infrared region.

Table B1. Spectral bands for kCARTA

Band (cm ⁻¹)	Point Spacing (cm ⁻¹)	Band center (μm)	number of files
15-30	0.00005	444.4	30
30-50	0.00010	250.0	20
50-80	0.00015	153.8	20
80-140	0.00025	90.9	28
140-300	0.00050	45.4	34
300-500	0.00100	25.0	21
500-605	0.00150 <u>0.00050</u>	18.1	07-21
605-2830 <u>605-880</u> *	<u>0.00050</u>	<u>14.18</u>	<u>40</u>
<u>805-2830</u> *	0.00250	5.8 <u>5.5</u>	89-81
2830-3550	0.00250	3.1	30
3550-5550	0.00100	2.2	21
5550-8250	0.01500	1.4	19
8250-12000	0.02500	0.98	16
12000-25000	0.05000	0.54	26
25000-44000	0.10000	0.29	19

Table B2: kCARTA features; * indicates currently only available in the f90 version

Feature	Default	Options
<u>SPECTROSCOPY</u>		
(1) IR Database	HITRAN 2016	HITRAN 2012, GEISA 2015
(2) Resolution	<u>0.0005</u> /0.0025 cm ⁻¹	can make other resolutions
(3) Molecular gases	HITRAN ID 1-42	choose some
(4) Cross-section gases	HITRAN (CFCs etc)	choose some
(5) Water continuum	MT-CKD 3.2	e.g. MT-CKD 1.0, 2.5
(6) CO ₂ line mixing	from LBLRTM -LBLRTM v12.8	UMBC-LBL line mixing
(7) CO ₂ /H ₂ O, CO ₂ /N ₂ CIA*	off	Hartmann and Tran*
(8) CH ₄ line mixing	from LBLRTM -LBLRTM v12.8	None (voigt)
(9) O ₂ and N ₂	HITRAN 2016 and LBLRTM -LBLRTM v1.28 continuum	
(10) NLTE	line by line *	SARTA approximation
(11) Uncompressiom	linear	spline
<u>RADIATIVE TRANSFER</u>		
(1)Temperature variation	Constant -Linear in τ^*	<u>Constant</u>

Continued on next page

Table B2 – Continued from previous page

Feature	Default	Options
(2) Background thermal	acos(3/5) in upper layers, accurate angle lower layers	acos(3/5) all layers gauss quadrature*
(3) Background thermal	lambertian	
Surface reflection	$(1 - \epsilon_s(\nu))/\pi$	
(4) Solar reflection	user specified	
(5) Ray tracing	Spherical atmosphere, $n=1$	n varies*
(6) Direction	<u>upwelling</u>	downwelling upwelling
(7) Solar	from tables	use 5600 K
(8) Jacobians	100 layer T, WV , weighting functions acos(3/5) backgrnd thermal	column jacs
(9) Fluxes*	upwell, downwell	Heating rates
RADIATIVE TRANSFER	ALL SKY	
(1) TwoSlab Cloud model*	PCLSAM PCLSAM	fluxes and jacobians
(2) couple to LBLDIS*		

Appendix C: ~~PCLSAM~~ scattering algorithm

600 The spline versus linear temperature interpolation differences, as tested on 49 regression profiles, are 0.0004 ± 0.0040 K, with a maximum absolute difference of 0.342 K (in the 15 μm region).

~~The PCLSAM~~

Appendix C: ~~PCLSAM~~ scattering algorithm

605 The PCLSAM scattering algorithm for longwave radiances has applications ranging from dust retrievals (De Souza-Machado et al., 2010), to modeling the effects of clouds on sounder data (Matricardi, 2005; Vidot et al., 2015). This scattering model changes the extinction optical depth from $k(\nu)$ to a parametrized number $k_{eff.extinction}^{scatterer}(\nu)$ (Chou et al., 1999), and is designed for cases of the single scattering albedo ω being much less than 1, such as in the thermal infrared, where ω for cirrus and water droplets and aerosols is typically on the order of 0.5.

Since $k_{eff.extinction}^{scatterer}(\nu)$ is now effectively the absorption due to the cloud or aerosol, for each layer i that contains scatterers we replace the gas absorption optical depth with the total absorption optical depth

$$610 \quad k_{total}(\nu) = k_{atm}^{gases}(\nu) + k_{eff.extinction}^{scatterer}(\nu) \quad (C1)$$

where (Chou et al., 1999) $k_{eff.extinction}^{scatterer}(\nu) = k_{extinction}^{scatterer}(\nu) \times (1 - \omega(\nu))(1 - b(\nu))$

where (Chou et al., 1999) $k_{eff.extinction}^{scatterer}(\nu) = k_{extinction}^{scatterer}(\nu) \times (1 - \omega(\nu))(1 - b(\nu))$ and the backscatter $b(\nu) = (1 - g(\nu))/2$, with $g(\nu)$ being the asymmetry factor. Using this for every layer containing scatterers, the radiative transfer algorithm is now the same as clear sky radiative transfer, with very little speed penalty.

615 kCARTA is capable of using a TwoSlab (De Souza-Machado et al., 2018) cloud representation scheme for use with PCLSAM. This allows for non unity fractions for up to two clouds, so that radiative transfer then assumes the total radiance is a sum of four radiance streams (clear, cloudy cloud 1, cloud 2 and the cloud overlap) weighted appropriately :

$$r(\nu) = c_{overlap}r^{(12)}(\nu) + c_1r^{(1)}(\nu) + c_2r^{(2)}(\nu) + f_{clr}r^{clr}(\nu) \quad (C2)$$

With this model kCARTA allows the user to specify upto up to two types of scatterers in the atmosphere (ice/water, ice/dust, water/dust or even ice/ice, water/water, dust/dust); the two scatterers are placed in separate "slabs" which occupy complete AIRS layers and are specified by cloud top/bottom pressure (in millibars), cloud amount (in g/m²), cloud effective particle diameter (in μm). After the computations are done, all five radiances are output when two clouds are defined (overlap, two clouds separately, clear, and the weighted sum), and three radiances if only one cloud is defined (one cloud, clear, weighted sum).

625 Analytic jacobians for temperature, gas amounts, and cloud micro-physical parameters (effective size and loading) can also be computed, as can be fluxes and associated heating rates, though the slab boundaries could introduce spikes in the heating rate profiles.

630 ~~Matlab routines~~ kCARTA does not have built-in multiple scattering capabilities to handle for example Rayleigh scattering in the ultra-violet. To handle this we have written Matlab routines to read in kCARTA optical depths ~~output and break them into separate files, which can be piped into LBLDIS and pipe them into~~ LBLDIS (Turner et al., 2003; Turner, 2005), a code that merges optical depths and scattering using the extensively tested Discrete Ordinates Radiative Transfer (DISORT) (Stamnes et al., 1988) algorithm.

Author contribution

Sergio DeSouza-Machado prepared the manuscript with contributions from all (living) co-authors. The initial compressed database coding and testing was done by L. Strow, H. Motteler and S. Hannon. Following this deS-M wrote the Fortran and Matlab wrapper codes for clear sky radiative transfer and jacobians, which were tested and validated by the other authors. Scattering and flux capabilities were added and tested by deS-M.

Competing interests

The authors declare that they have no conflict of interest.

640 **Acknowledgments**

We thank the anonymous reviewers whose comments/suggestions helped improve this manuscript. This work was supported in part by NASA grant number NNG04GG03G-2. Dave Tobin of UW-Madison helped with UMBC-LBL CO₂ line-mixing code and modifying the water continuum coefficients. Dave Edwards of NCAR provided the GENLN2 line-by-line code to compare kCARTA against. Both Dave Edwards and Manuel Lopez-Puertas of the Instituto de Astrofísica de Andalucía (Spain) contributed to the NLTE portions of the code. Optical depth and flux comparisons against LBLRTM were facilitated by Eli Mlawer (Atmospheric and Environmental Research, Lexington MA). ~~The impact of spectroscopic uncertainty to BTs at the TOA were carried out partly for the ITOVS Radiative Transfer Working Group, of which Marco Matricardi (ECMWF) is the leader. Iouli Gordon (Harvard-Smithsonian) suggested how to tweak the uncertainties when the indices were 0, 1, 2, as did Brian Drouin (JPL) for ozone line strengths.~~ while Guido Masiello (University of Basilicata, Italy) helped with the radiance inter-comparisons.

645

650

References

- Achard, V.: Trois problemes clés de l'analyse de la structure thermodynamique de l'atmosphère par satellite : mesure du contenu en ozone, classification de masses d'air : modelisation heper rapide du transfert radiatif, Ph.D. thesis, University Paris, available from LMD, Ecole Polytechnique, 91128 Palaiseau, France, 1991.
- 655 Aumann, H., Chahine, M., Gautier, C., Goldberg, M., Kalnay, E., McMillin, L., Revercomb, H., Rosenkranz, P., Smith, W., Staelin, D., Strow, L., and Susskind, J.: AIRS/AMSU/HSB on the Aqua Mission: Design, Science Objectives, Data Products and Processing Systems, *IEEE Trans. Geosci. Remote Sens.*, 41, 253–264, 2003.
- Birk, M., Wagner, G., ordon, I., and Drouin, B.: Ozone intensities in the rotational bands, *J. Quant. Spectrosc. Rad. Trans.*, 226, 60–85; <https://doi.org/10.1016/j.jsqrt.2019.01.004>, 2019.
- 660 Buehler, S., Eriksson, P., and Lemke, O.: Absorption lookup tables in the radiative transfer model ARTS, *J. Quant. Spectrosc. Rad. Trans.*, 112, 1559–1567; doi:10.1016/j.jsqrt.2011.03.008, 2011.
- Chou, M.-D., Lee, K.-T., Tsay, S.-C., and Fu, Q.: Parameterization for Cloud Longwave Scattering for use in Atmospheric Models, *J. Climate*, 12, 159–169, 1999.
- Clerbaux, C., Boynard, A., Clarisse, L., George, M., Hadji-Lazarro, J., Herbin, H., Hurtmans, D. Pommier, M., Razavi, A., Turquety, S., 665 Wespes, C., and Coheur, P.-F.: Monitoring of atmospheric composition using the thermal infrared IASI/MetOp sounder, *Atmos. Chem. and Phys.*, 9, 6041–6054, doi:10.5194/acp-9-6041-2009, 2009.
- Clough, S. and Iacono, M. J.: Line by line calculation of atmospheric fluxes and cooling rates.2. Application to Carbon-Dioxide,Ozone , Methane, Nitrous-Oxide and the Halocarbons, *J. Geophys. Res. A*, 100, D8, 16 519–16 535, 1995.
- Clough, S., Kneizys, F., Davies, R., Gamache, R., and Tipping, R.: Theoretical line shape for H₂O vapour; Application to the continuum, in: 670 Atmospheric water vapour, edited by Deepak, A., Wilkerson, T., and Rhunke, L., pp. 25–46, Academic Press, NY, 1980.
- Clough, S., Shephard, M., Mlawer, E., Delamere, J., Iacono, M. J., Cady-Pereira, K., Boukabara, S., and Brown, P.: Atmospheric radiative transfer modeling : a summary of the AER codes, *J. Quant. Spectrosc. Rad. Trans.*, 91, 233–244doi:10.016/j.jsqrt2004.05.058, 2005.
- Clough, S. A., Kneizys, F. X., and Davies, R. W.: Line Shape and the Water Vapor Continuum, *Atmos. Res.*, 23, 229–241, 1989.
- Clough, S. A., Iacono, M. J., and Moncet, J. L.: Line-by-line calculations of atmospheric fluxes and cooling rates: application to water vapor, 675 *J.Geophys.Res.*, 97, 15,761–15,785, 1992.
- De Souza-Machado, S., Strow, L. L., Tobin, D., Motteler, H., and Hannon, S.: UMBC-LBL: An Algorithm to Compute Line-by-Line Spectra, Tech. rep., University of Maryland Baltimore County, Department of Physics, <http://asl.umbc.edu/rta/lbl.html>, 2002.
- De Souza-Machado, S., Strow, L. L., Motteler, H., Hannon, S., Lopez-Puertas, M., Funke, B., and Edwards, D.: Fast Forward Radiative Transfer Modeling of 4.3 um Non-Local Thermodynamic Equilibrium effects for the Aqua/AIRS Infrared Temperature Sounder, *Geophys. Res. Lett.*, 34, doi:10.1029/2006GL026 684,L01 802, 2007.
- 680 De Souza-Machado, S., Strow, L. L., Imbiriba, B., McCann, K., Hoff, R., Hannon, S., Martins, J., Tanré, D., Deuzé, J., Ducos, F., and Torres, O.: Infrared retrievals of dust using AIRS: comparisons of optical depths and heights derived for a North African dust storm to other collocated EOS A-Train and surface observations, *J. Geophys. Res.*, 115, doi:10.1029/2009JD012 842,D15 201, 2010.
- De Souza-Machado, S., Strow, L. L., Tangborn, A., Huang, X., Chen, X., Liu, X., Wu, X., and Yang, Q.: Single-footprint retrievals for AIRS 685 using a fast TwoSlab cloud-representation model and the SARTA all-sky infrared radiative transfer algorithm, *Atmos. Meas. Tech.*, 11, 529–550, <https://doi.org/10.5194/amt-11-529-2018>, 2018.

- Drouin, B., Crawford, T., and Yu, S.: Validation of ozone intensities at 10 um with THz spectrometry, *J. Quant. Spectrosc. Rad. Trans.*, 203, 282–292; <https://doi.org/10.1016/j.jqsrt.2017.06.035>, 2017.
- Dudhia, A.: The Reference Forward Model (RFM), *J. Quant. Spectrosc. Rad. Trans.*, 186, 243–253, 2017.
- 690 Edwards, D.: GENLN2: A General Line-by-Line Atmospheric Transmittance and Radiance Model, *NCAR Technical Note 367+STR*, National Center for Atmospheric Research, Boulder, Colo., 1992.
- Edwards, D. P., Lopez-Puertas, M., and López-Valverde, M.: Non LTE Studies of 15 um bands of CO₂ for Atmospheric Remote Sensing, *J. Geophys. Res.*, 98, 14 955–14 977, 1993.
- Edwards, D. P., Lopez-Puertas, M., and Gamache, R.: The Non LTE CO₂ Correction to the Vibrational Component of the Internal Partition Sum
695 for Atmospheric Calculations, *J. Quant. Spectrosc. Rad. Trans.*, 59, 423–436, 1998.
- Farmer, C. B. and Norton, R.: Atlas of the Infrared Spectrum of the Sun and the Earth Atmosphere from Space. Volume I, The Sun, NASA JPL publication 1224, NASA, Pasadena, CA, 1989.
- Farmer, C. B., Raper, O., and O’Callaghan, F.: Final report on the first flight of the ATMOS instrument during the Spacelab 3 mission, April 29 through May 6, 1985, JPL publication 87–32, Jet Propulsion Laboratory, Pasadena, CA, 1987.
- 700 Gambacorta, A.: The NOAA Unique CrIS/ATMS Processing System (NUCAPS): Algorithm Theoretical Basis Documentation, Tech. rep., NCWCP, http://www.ospo.noaa.gov/Products/atmosphere/soundings/nucaps/docs/NUCAPS_ATBD_20130821.pdf, 2013.
- Goody, R. and Yung, Y.: Atmospheric Radiation: Theoretical Basis, Oxford University Press, 1989.
- Gordon, I.: private communication, 4/18, HITRAN line parameter uncertainties, 2018.
- Gordon, I., Rothman, L., Hill, C., Kochanov, R., and Tan, Y. e. a.: The HITRAN 2016 molecular spectroscopic database, *J. Quant. Spectrosc. Rad. Trans.*, 203, 3–69; <https://doi.org/10.1016/j.jqsrt.2017.06.038>, 2017.
- 705 Han, Y., Revercomb, H., Crompton, M., Strow, L., Chen, Y., and Tobin, D.: Suomi NPP CrIS measurements, sensor data record algorithm, calibration and validation activities, and record data quality, *J. Geophys. Res.*, 118, doi:10.1002/2013JD020 344, 2013.
- Hartmann, J.-M., Boulet, C., Tran, D., Tran, H., and Baranov, Y.: Effect of humidity on the absorption continua of CO₂ and N₂ near 4 um : calculations, comparisons with measurements, consequences on atmospheric spectra, *J. Chem. Phys.*, 148, 54 304, 2018.
- 710 Hoffman, L. and Alexander, M.: Retrieval of stratospheric temperatures from Atmospheric Infrared Sounder radiance measurements for gravity wave studies, *J. Geophys. Res.*, 114, D07 105; doi:10.1029/2008JD011 241, 2009.
- Husson, N., Armante, R., Scott, N., Chedin, A., Crepeau, L., Boitamine, C., Bouhdaoui, A., Crevoisier, C., Capelle, V., Boone, C., Poulet-Croviser, N., Barbe, A., Benner, C., Boudon, V., Brown, L., Buldyreva, J., Campargue, A., L.H., C., Makie, A., and et. al.: The 2015 edition of the GEISA spectroscopic database, *J. Mol. Spectr.*, 327, 31–72; <https://doi.org/10.1016/j.jms.2016.06.007>, 2015.
- 715 Lamouroux, J., Tran, H., Laraia, A. L., Gamache, R. R., Rothman, L. S., Gordon, I. E., and Hartmann, J.-M.: Updated database plus software for line-mixing in CO₂ infrared spectra and their test using laboratory spectra in the 1.5–2.3 um region, *J. Quant. Spectrosc. Rad. Trans.*, 111, 2321–2331; [10.1016/j.jqsrt.2010.03.006](https://doi.org/10.1016/j.jqsrt.2010.03.006), 2010.
- Lamouroux, J., Rogalia, L., Thomas, X., Vander Auwera, J., Gamache, R., and Hartmann, J.-M.: CO₂ line-mixing database and software update and its tests in the 2.1 um and 4.3 um regions, *J. Quant. Spectrosc. Rad. Trans.*, 151, 88–96; <https://doi.org/10.1016/j.jqsrt.2014.09.017>, 2015.
- 720 Liou, K.: An Introduction to Atmospheric Radiation, Academic Press, 1980.
- Liu, X., Smith, W., Zhou, D., and Larar, A.: Principal component based radiative transfer model for hyperspectral sensors : theoretical concepts, *Appl. Opt.*, 45, 201–209, 2006.
- Lopez-Puertas, M. and Taylor, F.: NONLTE Radiative Transfer in the Atmosphere, World Scientific Publishing, 2001.

- 725 Matricardi, M.: The inclusion of aerosols and clouds in RTIASI, the ECMWF fast radiative transfer model for the infrared atmospheric sounding interferometer, 2005.
- McClatchey, R., Fenn, R., Selby, J., Volz, F., and Garing, J.: Optical properties of the atmosphere, Tech. Rep. AFCRL-72-0497, AFGL(OPI), Hanscom AFB, MA 01731, 1972.
- Mlawer, E. J.: Private communication, 2016.
- 730 Mlawer, E. J., Payne, V. H., Moncet, J.-L., Delamere, J., Alvarado, M., and Tobin, D.: Development and recent evaluation of the MT_CKD model of continuum absorption, *Phil. Trans. Roy. Soc. A*, 370, 1–37, doi:10.1098/rsta.2011.0295, 2012.
- Nalli, N., Smith, W., and Liu, Q.: Angular Effect of Undetected CLOUDS in Infrared Window Radiance Observations : Aircraft Experimental Analysis, *J.Atmos.Sci.*, 73, 1987–2011, DOI: 10.1175/JAS-D-15-0262.1, 2016.
- Niro, F., Jucks, K. W., and Hartmann, J. M.: Spectra calculations in central and wing regions of CO₂ IR bands between 10 and 20 μm :
 735 Software and database for the computation of atmospheric spectra, *J. Quant. Spectrosc. Rad. Trans.*, 95, 469–481, 2005.
- Rodgers, C.: *Inverse Methods for Atmospheric Sounding*, World Scientific, Singapore, 2000.
- Rothman, L. S., Jacquemart, J., Barbe, C., Benner, D., Birk, M., Brown, L., Carleer, M., Chackerian, C., Chance, K., Coudert, L., Dana, V., Devi, V., Flaud, J.-M., Gamache, R., Goldman, A., Hartmann, J.-M., Juck, K., Maki, A., Mandin, J.-Y., Massie, S., Orphal, J., Perrin, A., Rinsland, C., Smith, M., Tennyson, J., Tolchenov, R., Toth, R., Vander Auwera, J., Varanasi, P., and Wagner, G.: The HITRAN 2004
 740 molecular spectroscopic database, *J. Quant. Spectrosc. Rad. Trans.*, 96, 139–204, 2005.
- Rothman, L. S., Gordon, I., Babikov, Y., Barbe, A., Benner, D., and Bernath, P. e. a.: The HITRAN 2012 molecular spectroscopic database, *J. Quant. Spectrosc. Rad. Trans.*, 130, 4–50, 2013.
- Saunders, R., Matricardi, M., and Brunel, P.: An improved fast radiative transfer model for the assimilation of satellite radiance observations, *Quart.J.Roy.Meteorol.Soc.*, 125, 1407–1425, 1999.
- 745 Schreier, F., Garcia, S., Hedelt, P., Hess, M., Mendrok, J., Vasquez, M., and Xu, J.: GARLIC — A general purpose atmospheric radiative transfer line-by-line infrared-microwave code: Implementation and evaluation, *J. Quant. Spectrosc. Rad. Trans.*, 137, 29–50, 2014.
- Stamnes, K., Tsay, S.-C., Wiscombe, W., and Jayaweera, K.: Numerically Stable Algorithm for discrete ordinate method Radiative Transfer in multiple scattering and emitting layered media, *Appl. Opt.*, 27, 2502–2509, 1988.
- Strow, L., Motteler, H., Benson, R., Hannon, S., and De Souza-Machado, S.: Fast Computation of Monochromatic Infrared Atmospheric
 750 Transmittances using Compressed Look-Up Tables, *J. Quant. Spectrosc. Rad. Trans.*, 59, 481–493, 1998.
- Strow, L., Hannon, S., DeSouza-Machado, S., Tobin, D., and Motteler, H.: An Overview of the AIRS Radiative Transfer Model, *IEEE Transactions on Geosciences and Remote Sensing*, 41, 303–313, 2003.
- Strow, L. L. and Pine, A. S.: Q-branch line mixing in N₂O: Effects of ℓ -type doubling, *J. Chem. Phys.*, 89, 1427, 1988.
- Susskind, J., Barnett, C., and Blaisdell, J.: Atmospheric and Surface Parameters from Simulated AIRS/AMSU/HSB Sounding Data: Retrieval
 755 and Cloud Clearing Methodology, *Adv. Space. Sci.*, 21, 369–384 doi:10.1016/S0273-1177(97)00916-2, 1998.
- Tjemkes, S., Patterson, T., Rizzi, R., Shephard, M., Clough, S., Matricardi, M., Haigh, J., Hopfner, M., Payan, S., Trotsenko, A., Scott, N., Rayer, P., Taylor, J., CLerbaux, C., Strow, L., DeSouza-Machado, S., Tobin, D., and Knuteson, R.: The ISSWG Line-by-line Intercomparison Experiment, *J. Quant. Spectrosc. Rad. Trans.*, 77, 433, 2002.
- Tobin, D. C., Strow, L. L., Lafferty, W. J., and Olson, W. B.: Experimental Investigation of the Self- and N₂- Broadened Continuum within
 760 the ν_2 Band of Water Vapor, *Appl. Opt.*, 35, 1, 1996.

- Tran, H., Flaud, P.-M., Gabard, T., Hase, F., Von Clarmann, T., Camy-Peyret, C., Payan, S., and Hartmann, J.-H.: Model, Software and database for line-mixing effects in the v3 and v4 bands of CH₄ and tests using laboratory and planetary measurements. I. N₂ (and air) broadening and the Earth atmosphere, *J. Quant. Spectrosc. Rad. Trans.*, 101, 284–305, 2006.
- Tran, H., Turbet, M., Chelin, P., and Landsheere, X.: Measurements and modeling of absorption by CO₂+H₂O mixtures in the spectral region beyond the CO₂ v3 bandhead, *Icarus*, 306, 116–121, 2018.
- 765 Turner, D.: Arctic mixed-phase cloud properties from AERI-lidar observations: Algorithm and results from SHEBA, *J.Appl. Met.*, 44, 427–444, 2005.
- Turner, D., Ackerman, S., Baum, B., Revercomb, H., and Yang, P.: Cloud Phase Determination using ground based AERI observations at SHEBA, *J.Appl. Met.*, 42, 701–715, 2003.
- 770 Van Vleck, J. H. and Huber, D. L.: Absorption, emission, and linebreadths: A semihistorical perspective, *Rev. Mod. Phys.*, 49, 939, 1977.
- Vidot, J., Baran, A., and Brunel, P.: A new ice cloud parameterization for infrared radiative transfer simulation of cloudy radiances: Evaluation and optimization with IIR observations and ice cloud profile retrieval products, *J. Geophys. Res.*, 120, doi:10.1002/2015JD023462, 6937–6951, 2015.
- Vincent, R. and Dudhia, A.: Fast radiative transfer using monochromatic look-up tables, *J. Quant. Spectrosc. Rad. Trans.*, 186, 254–264, <https://doi.org/10.1016/j.jqsrt.2016.04.011>, 2017.
- 775 Zorn, S., von Clarmann, T., Echle, G., Funke, B., Hase, F., Hopfner, M., Kemnitzer, H., Kuntz, M., and Stiller, G.: KOPRA: Analytic expressions for modelling radiative transfer and instrumental effects, Tech. rep., Karlsruhe University, Germany, https://www.imk-asf.kit.edu/downloads/SAT/kopra_docu_part02.pdf, 2002.